NEUROSCIENCE

GABARAPs dysfunction by autophagy deficiency in adolescent brain impairs $GABA_A$ receptor trafficking and social behavior

Kelvin K. Hui[1], Noriko Takashima[1], Akiko Watanabe[2], Thomas E. Chater[3], Hiroshi Matsukawa[1,4], Yoko Nekooki-Machida[1], Per Nilsson[5,6], Ryo Endo[1], Yukiko Goda[3], Takaomi C. Saido[5], Takeo Yoshikawa[2], Motomasa Tanaka[1]*

Dysfunctional mTOR signaling is associated with the pathogenesis of neurodevelopmental and neuropsychiatric disorders. However, it is unclear what molecular mechanisms and pathogenic mediators are involved and whether mTOR-regulated autophagy continues to be crucial beyond neurodevelopment. Here, we selectively deleted *Atg7* in forebrain GABAergic interneurons in adolescent mice and unexpectedly found that these mice showed a set of behavioral deficits similar to *Atg7* deletion in forebrain excitatory neurons. By unbiased quantitative proteomic analysis, we identified γ-aminobutyric acid receptor–associated protein-like 2 (GABARAPL2) to differentially form high–molecular weight species in autophagy-deficient brains. Further functional analyses revealed a novel pathogenic mechanism involving the p62-dependent sequestration of GABARAP family proteins, leading to the reduction of surface $GABA_A$ receptor levels. Our work demonstrates a novel physiological role for autophagy in regulating GABA signaling beyond postnatal neurodevelopment, providing a potential mechanism for the reduced inhibitory inputs observed in neurodevelopmental and neuropsychiatric disorders with mTOR hyperactivation.

INTRODUCTION

Recent genetic studies indicate the involvement of dysregulated mechanistic target of rapamycin (mTOR) signaling, a central regulator of various cellular processes including protein translation, actin dynamics, and autophagy, in neurodevelopmental [e.g., autism spectrum disorder (ASD) and intellectual disability (ID)] and neuropsychiatric [e.g., schizophrenia (SZ) and bipolar disorder (BD)] disorders (*1*). For instance, mutations in several genes such as *TSC1*, *TSC2*, *NF1*, and *PTEN* result in hyperactivated mTOR and are associated with multiple dimensions of psychiatric symptoms including social deficits. Many behavioral deficits observed in these models can be alleviated with mTOR inhibitors such as rapamycin, thus highlighting the predominant contribution of mTOR dysregulation to the abnormalities. Most studies to date have focused on delineating the consequences of hyperactivated mTOR and its influence on protein synthesis and synaptic plasticity (*2*, *3*). Yet, how the dysregulation of other downstream signaling pathways like autophagy may contribute to the manifestation of behavioral abnormalities in neurodevelopmental and neuropsychiatric disorders remains poorly understood (*4*). Moreover, the mediators and molecular mechanisms therein remain unclear.

Deficits in γ-aminobutyric acid (GABA) signaling have also been closely implicated in the pathogenesis of neurodevelopmental and neuropsychiatric disorders. For example, Prader-Willi syndrome, Angelman syndrome, and cases of SZ are associated with 15q11-q13 copy number variations, a chromosomal region that encodes for multiple subunits of the $GABA_A$ receptor including *GABRB3*, *GABRA5*, and *GABRG3* (*5*). Postmortem studies using brain samples from ASD (*6*) and SZ (*7*) patients have revealed alterations in glutamic acid decarboxylase (GAD65 and GAD67) expression, further implicating defective GABAergic signaling in pathogenesis. GABA neurotransmission was also highlighted in BD pathology, as polymorphisms in multiple $GABA_A$ receptor subunits have been identified in BD patients (*8*). Furthermore, deletion of a number of genes associated with neurodevelopmental and neuropsychiatric disorders in mice has revealed specific deficits in the development of GABAergic interneurons or GABA neurotransmission (*9*, *10*). Collectively, there is overwhelming evidence that links GABA signaling deficits to neurodevelopmental and neuropsychiatric disorders.

Despite the wealth of experimental evidence highlighting the critical roles of both mTOR and GABAergic signaling in the pathogenesis of neurodevelopmental and neuropsychiatric disorders, we know little about whether they may converge and modulate neuronal functions beyond postnatal neurodevelopment. In this study, we specifically impaired autophagic function in forebrain GABAergic interneurons of adolescent mice to evaluate the impact of this major downstream pathway regulated by mTOR and revealed a common pathogenic mechanism by which autophagy deficiency affects GABA signaling in both GABAergic inhibitory neurons and excitatory neurons.

RESULTS

Overlapping behavioral deficits displayed by mice with autophagy deficiency in forebrain GABAergic interneurons or excitatory neurons

To evaluate the contribution of disrupted mTOR-autophagic signaling in forebrain GABAergic interneurons to the manifestation of behavioral abnormalities associated with neurodevelopmental or neuropsychiatric disorders, we generated and examined the conditional deletion of *Atg7* by Dlx5-creERT2. Alterations in mTOR signaling

[1]Laboratory for Protein Conformation Diseases, RIKEN Center for Brain Science, Wako, Saitama 351-0198, Japan. [2]Laboratory for Molecular Psychiatry, RIKEN Center for Brain Science, Wako, Saitama 351-0198, Japan. [3]Laboratory for Synaptic Plasticity and Connectivity, RIKEN Center for Brain Science, Wako, Saitama 351-0198, Japan. [4]Laboratory for Behavioral Genetics, RIKEN Center for Brain Science, Wako, Saitama 351-0198, Japan. [5]Laboratory for Proteolytic Neuroscience, RIKEN Center for Brain Science, Wako, Saitama 351-0198, Japan. [6]Department of Neurobiology, Care Sciences and Society, Karolinska Institutet, Huddinge 141 57, Sweden.
*Corresponding author. Email: motomasa.tanaka@riken.jp

were previously shown to affect neurogenesis and migration of forebrain GABAergic interneurons (*11*), and autophagy was proposed recently to disrupt synaptic pruning (*4*, *12*). Thus, *Atg7* deletion was initiated in adolescent mice to exclude those effects to specifically examine the consequence of autophagy deficiency in mature GABAergic interneurons. We first confirmed the reduction of Atg7 expression and observed the accumulation and aggregate formation of p62, an adaptor protein responsible for recognizing and loading of cargo substrates into autophagosomes, as a classical marker of autophagy suppression/disruption (*13*, *14*) in all major classes of forebrain GABAergic interneurons without detectable neurodegeneration at 6- to 8-month post-Cre recombinase induction, when all experiments were performed (Fig. 1, A and B, and fig. S1, A to D). We then performed a battery of behavioral tests (see Methods for details) on Dlx5-creERT2 *Atg7* conditional knockout (cKO) and control (Dlx5-control) mice and examined whether their phenotypes in each test are similar to or different from those in CaMKII-cre *Atg7* cKO/control (CaMKII-control) mice. We found that both *Atg7* cKO mice shared a set of behavioral abnormalities including reduced social interaction, as examined by resident-intruder (Fig. 1, C and D) and three-chamber social interaction tests (Fig. 1, E and F), disturbed nesting behavior (Fig. 1, G and H), and increased anxiety as demonstrated by elevated plus maze (Fig. 1, I and J). In contrast, no deficits in motor function, exploratory activity, or stress vulnerability were observed for both *Atg7* cKO mice by open-field activity test and tail suspension test (fig. S1, E to H).

Recent studies suggested that behavioral abnormalities in mice with autophagy deficiency in forebrain excitatory neurons or microglia were caused by synaptic pruning deficits during postnatal neurodevelopment; however, the molecular mechanism was not fully examined (*4*, *12*). As we have observed similar behavioral deficits in Dlx5-cre ERT2 *Atg7* cKO mice, although *Atg7* deletion was initiated beyond the peak of synaptic pruning in adolescent mice, we asked whether this finding was specific to GABAergic interneurons or whether conditional *Atg7* deletion in forebrain excitatory neurons at a similar stage may also disrupt social behaviors. To test this hypothesis, we performed adeno-associated virus (AAV) injections to locally delete *Atg7* in excitatory neurons of the medial prefrontal cortex (mPFC) of adolescent $Atg7^{flox/flox}$ mice (12 weeks old) (fig. S1, I and J), a brain region previously shown to be critical for social interactions (*15*, *16*). We observed that mice with autophagy deficiency, specifically in mPFC excitatory neurons, similarly exhibited social interaction deficits compared to controls (Fig. 1K), while other behavioral abnormalities were not observed (Fig. 1, L and M, and fig. S1, K and L). Thus, autophagy in forebrain excitatory neurons continues to play an important role in regulating social behavior beyond postnatal development. Furthermore, despite deleting *Atg7* from distinct neuronal populations, the similar set of behavioral deficits observed in both *Atg7* cKO mice suggested that a common mechanism may be involved.

Aggregation and mislocalization of GABARAPs to $p62^+$ aggregates in autophagy-deficient neurons of Dlx5-creERT2 and CaMKII-cre *Atg7* cKO mice

We reasoned that because autophagy deficiency in neurons accumulates $p62^+$ and $ubiquitin^+$ aggregates (*17*), the soluble pool of affected proteins could be substantially reduced by enhanced protein aggregation and, consequently, be compromised in their functions. To identify proteins that were differentially aggregated into high–molecular weight species (>250 kDa) in *Atg7* cKO brains, we performed an unbiased quantitative proteomic screen by combining semidenaturing detergent agarose gel electrophoresis (SDD-AGE) (*18*) with spike-in stable isotope labeling of amino acids in mammals (SILAM) (Fig. 2A) (*19*). To maximize the sample size and homogeneity for reliable, quantitative mass spectrometric (MS) analysis, we carried out this experiment using cortical brain homogenates from CaMKII-cre *Atg7* cKO and control mice (6 months old). We specifically searched for proteins similar to p62, which were absent in the high–molecular weight fraction from control brains but had increased amounts in *Atg7* cKO brains (fig. S1B), because their functions may be most severely affected by autophagy deficiency. We identified 15 proteins that fit our criteria (SILAM score > 1.5 in both of two independent experiments) (Fig. 2, B and C, and fig. S2A). When we extended this experiment with *Atg7* cKO and control brains from other ages (3 and 12 months old), only three proteins including p62 consistently met the selection criteria (Fig. 2D and fig. S2B). Among them, we were interested in GABA receptor–associated protein-like 2 (GABARAPL2), which is involved in autophagy as an Atg8-like protein (*20*) and whose paralog GABARAP was suggested to mediate trafficking of $GABA_A$ receptors (*21*). However, the neuronal functions of GABARAP family proteins remain poorly understood, although they are all highly expressed in the brain (*22*). All three family members showed increased protein levels in *Atg7* cKO brains (Fig. 2E), in contrast to other Atg8-like proteins like LC3 that do not substantially accumulate under autophagy-deficient conditions (*17*). We next examined by native polyacrylamide gel electrophoresis (PAGE) whether the identification of GABARAPL2 in our MS-based screen was due to the increased amounts of GABARAPL2 in *Atg7* cKO brains or was actually caused by a change from its native conformation to high–molecular weight species. We found that, in addition to accumulating in *Atg7* cKO brains, the migration of GABARAPL2 and GABARAP under native conditions appears to have shifted to a high–molecular weight region (Fig. 2F), indicating potential changes in self-assembly or interactions with other proteins such as formation of homo-/hetero-oligomeric protein complexes. To gain further insights, we examined the subcellular localization of GABARAPL2 and its paralogs, GABARAPL1 and GABARAP, by immunofluorescence in Dlx5-creERT2, full, and mPFC-specific CaMKII-cre *Atg7* cKO mice. We found that all three proteins were sequestered into the $p62^+$ aggregates formed following *Atg7* deletion (Fig. 2, G to I, and fig. S2, C to J). The mislocalization of GABARAPs to $p62^+$ aggregates and their coaggregation, in addition to the observed shift from monomeric species to high–molecular weight complexes, suggest that the functions of GABARAPs could be compromised as a result of autophagy deficiency.

Because GABARAP was originally identified as a $GABA_A$ receptor–interacting protein (*23*) and suggested to mediate the trafficking of $GABA_A$ receptors (*21*), we examined whether surface expression of $GABA_A$ receptors may be altered in *Atg7* cKO mice. To this end, we performed in situ surface receptor biotinylation on striatal and hippocampal tissue dissected from Dlx5-creERT2 and CaMKII-cre *Atg7* cKO and control mice, respectively, to maximize sample homogeneity, as those tissues are predominantly populated by Cre recombinase–expressing $Dlx5^+$ or $CaMKII\alpha^+$ neurons. While no significant differences were observed for surface fractions of both α-amino-3-hydroxy-5-methyl-4-isoxazolepropionic acid (AMPA) and *N*-methyl-D-aspartate (NMDA) receptors, a specific reduction of surface $GABA_A$ receptors was detected in both tissues lacking *Atg7*

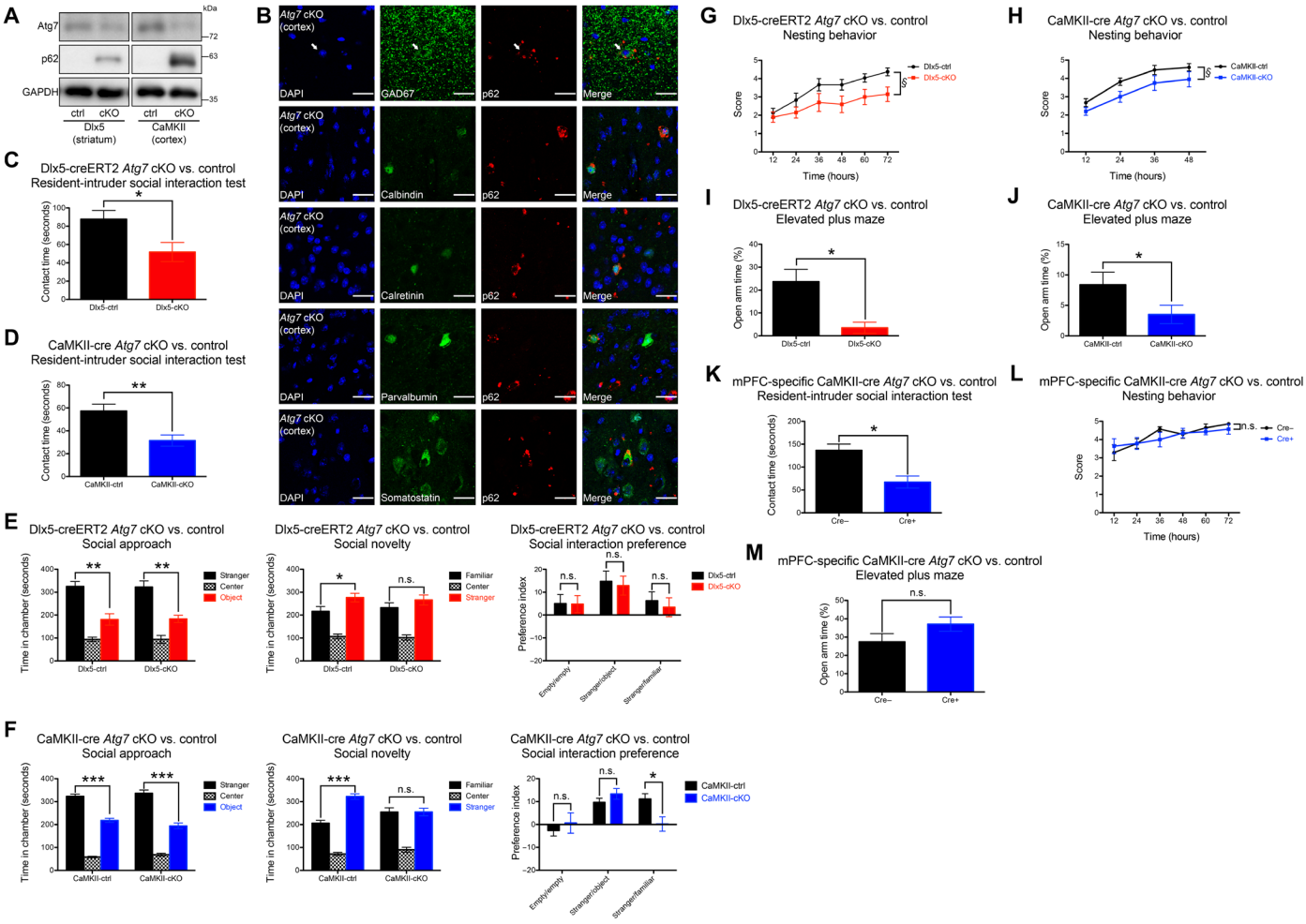

Fig. 1. Autophagy deficiency in forebrain GABAergic inhibitory or excitatory neurons resulted in an overlapping set of ASD-like behavioral deficits. (**A**) *Atg7* conditional deletion by Dlx5-creERT2 and CaMKII-cre led to increased p62 levels in affected brain regions. (**B**) $p62^{+}$ aggregate formation was observed in all major subclasses of cortical GABAergic interneurons of Dlx5-creERT2 *Atg7* cKO mice. (**C** and **D**) Resident-intruder social interaction test showed deficits in both Dlx5-creERT2 and CaMKII-cre *Atg7* cKO mice. $n = 10$ (Dlx5-control), $n = 8$ (Dlx5-cKO), $n = 16$ (CaMKII-control), $n = 16$ (CaMKII-cKO). (**E** and **F**) Three-chamber social interaction test revealed a difference in Dlx5-creERT2 and CaMKII-cre *Atg7* cKO mice for social novelty (middle) but not social approach (left). A social interaction preference index was also calculated, which showed a statistical significant difference for social novelty across genotypes for CaMKII-cre but not Dlx5-creERT2 *Atg7* cKO animals (right). $n = 12$ (Dlx5-control), $n = 10$ (Dlx5-cKO), $n = 16$ (CaMKII-control), $n = 16$ (CaMKII-cKO). (**G** and **H**) Deficits in nesting behavior were observed for both Dlx5-creERT2 and CaMKII-cre *Atg7* cKO mice. $n = 12$ (Dlx5-control), $n = 10$ (Dlx5-cKO), $n = 14$ (CaMKII-control), $n = 10$ (CaMKII-cKO). (**I** and **J**) Elevated plus maze showed that both Dlx5-creERT2 and CaMKII-cre *Atg7* cKO mice have increased anxiety. $n = 5$ (Dlx5-control), $n = 4$ (Dlx5-cKO), $n = 14$ (CaMKII-control), $n = 16$ (CaMKII-cKO). (**K**) Localized *Atg7* deletion in mPFC excitatory neurons in 12-week-old $Atg7^{flox/flox}$ mice led to deficits in social behavior as measured by the resident-intruder social interaction test. $n = 7$ animals per genotype. (**L** and **M**) mPFC-specific autophagy deficiency in excitatory neurons did not affect nesting or anxiety-related behaviors. $n = 7$ animals per genotype. Data are presented as means ± SEM. $^{*}P < 0.05$, $^{**}P < 0.01$, $^{***}P < 0.001$, unpaired two-tailed Student's *t* test; $^{§}P < 0.05$, between genotypes, two-way repeated-measures analysis of variance (ANOVA). n.s., not statistically significant.

(Fig. 3A and fig. S3A). Next, to investigate whether the reduced surface $GABA_A$ receptor levels would impair electrophysiological functions, we performed recordings of both miniature inhibitory and excitatory postsynaptic currents (mIPSC and mEPSC, respectively) from CA1 pyramidal cells (*Atg7* intact) of Dlx5-creERT2 *Atg7* cKO and control mice. We detected a significant increase in mIPSC frequency without any changes in amplitude (Fig. 3B), suggesting that autophagy deficiency in GABAergic interneurons enhanced GABA release onto their target cells. In contrast, mEPSC recordings showed no differences (fig. S3B), indicating that there were no non–cell-autonomous effects on excitatory neurons by *Atg7* deletion in GABAergic interneurons. Together, these results revealed that GABAergic interneurons in Dlx5-creERT2 *Atg7* cKO mice are potentially hyperactive, consistent with the lower surface expression of $GABA_A$ receptors and thus reduced inhibitory input. From these experiments, we revealed that GABARAPs were functionally compromised because of the formation of high–molecular weight species in autophagy-deficient neurons, which led to reduced trafficking of $GABA_A$ receptors in affected cells and altered GABAergic signaling in the brain.

Reduced GABARAPL2 function contributes to reduced $GABA_A$ receptor trafficking in autophagy-deficient cortical GABAergic interneurons

To examine the molecular mechanism underlying this observation in detail, we examined autophagy deficiency in vitro using cultured

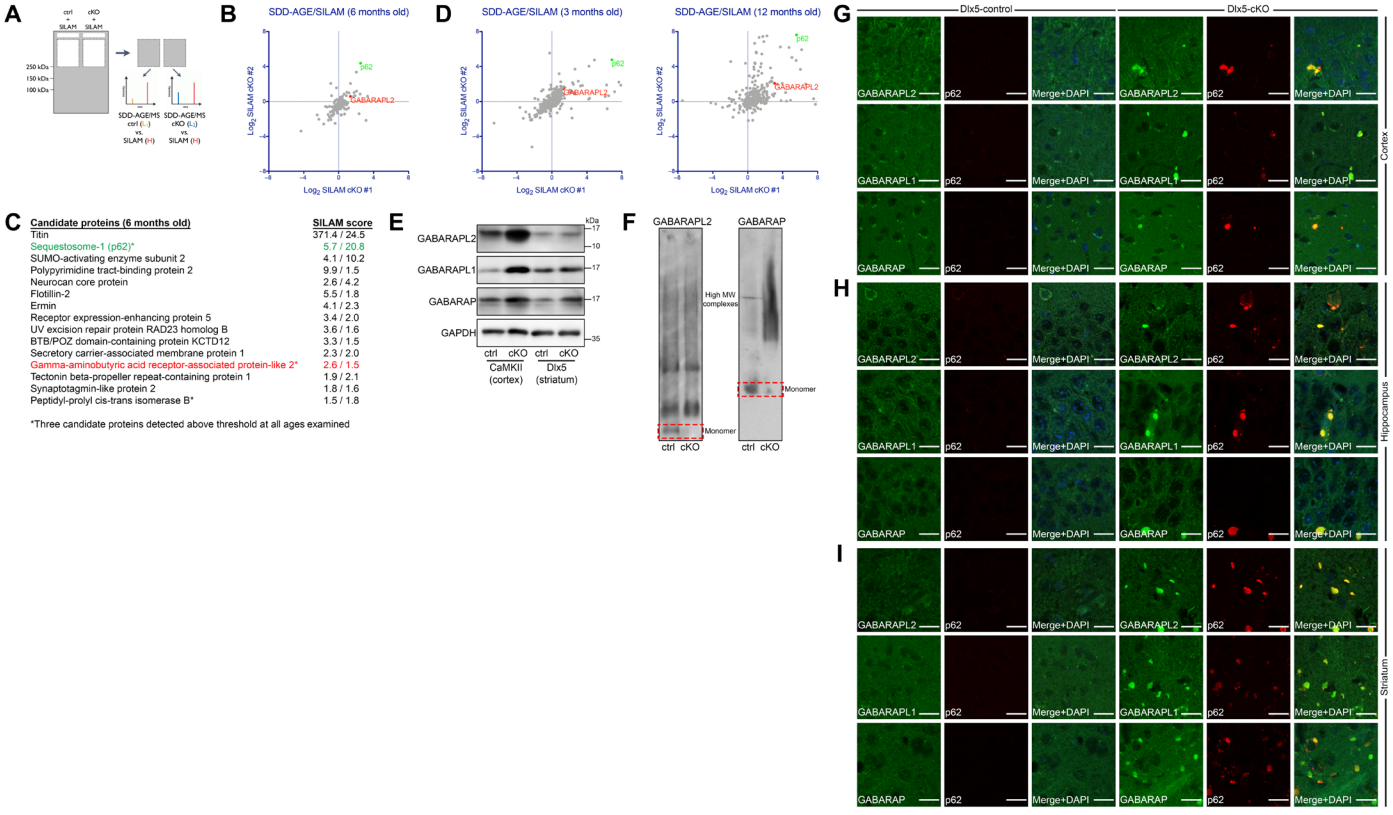

Fig. 2. Mislocalization and altered conformational status of GABARAPs in *Atg7* cKO brains. (**A**) Schematic diagram of SDD-AGE/SILAM experiment. (**B**) Abundance of proteins identified in high molecular weight fraction (>250 kDa) only in CaMKII-cre *Atg7* cKO but not control brains by SDD-AGE/SILAM experiments (6-month-old mice). (**C**) Candidate proteins meeting the selection criteria are listed with SILAM scores representing relative abundance to SILAM-labeled sample. Selection criteria are depicted schematically in fig. S2B. Candidate proteins identified by these criteria at all three ages examined are specifically marked by asterisks. (**D**) GABARAPL2 and p62 were consistently identified by SDD-AGE/SILAM in CaMKII-cre *Atg7* cKO brain homogenates at 3 months (left) and 12 months (right) of age. (**E**) p62-like accumulation of GABARAPs was observed in Dlx5-creERT2 and CaMKII-cre *Atg7* cKO mice. (**F**) Native PAGE analysis revealed shifts of GABARAPL2 and GABARAP into high–molecular weight (MW) complexes in the brains of CaMKII-cre *Atg7* cKO mice (cortex). (**G** to **I**) GABARAPs were observed to mislocalize to $p62^+$ aggregates in affected neurons of Dlx5-creERT2 *Atg7* cKO mice. Scale bars, 20 μm (G to I).

cortical GABAergic interneurons derived from the embryonic medial ganglionic eminence (MGE). Similar to autophagy-deficient brain tissue, we observed the accumulation of GABARAPs and p62 as a result of *Atg7* deletion (Fig. 4A). Consistent with results from in situ surface receptor biotinylation, we found a specific reduction of surface $GABA_A$ receptors in *Atg7* cKO GABAergic interneurons without alterations in the total protein level, while AMPA and NMDA receptors remained unchanged in both total and surface fractions (Fig. 4B and fig. S4A). We further confirmed the reduced surface expression of $GABA_A$ receptors by nonpermeable immunofluorescence staining. Using an antibody specific to the extracellular domain of $\beta_{2/3}$ subunit, we observed a reduction of surface-exposed $GABA_A$ receptors in autophagy-deficient GABAergic interneurons (Fig. 4C and fig. S4B). To directly assess whether the reduction of surface $GABA_A$ receptors in *Atg7* cKO neurons affected their activity, we recorded spontaneous action potentials from *Atg7* cKO and control neurons. Consistent with hyperactivity of GABAergic interneurons in the hippocampi of Dlx5-creERT2 *Atg7* cKO mice (Fig. 3B), we observed a significant increase in the frequency of spontaneous action potentials (Fig. 4D, top, and fig. S4C) in cultured *Atg7* cKO neurons without any changes in resting membrane potential (Fig. 4D, bottom).

While GABARAP was reported to mediate $GABA_A$ receptor trafficking (*21*), whether GABARAPL2 and GABARAPL1 also have this function has not been addressed. In particular, GABARAPL2 was previously reported to show no interaction with $GABA_A$ receptors or gephyrin, a scaffolding protein involved in clustering and stabilization of $GABA_A$ receptors (*24*). We first examined whether GABARAPL2 may also be involved with $GABA_A$ receptor trafficking by short hairpin RNA (shRNA)–mediated knockdown. As shown in Fig. 4E, *Gabarapl2* knockdown in wild-type (WT) GABAergic interneurons (fig. S4D) resulted in a significant reduction of surface $GABA_A$ receptors, indicating that it is also involved in $GABA_A$ receptor trafficking. Since GABARAPs, as Atg8 homologs, have the ability to bind to p62 (*25*), we hypothesized that the accumulated p62 in *Atg7* cKO neurons may outcompete their normal physiological interactors, such as gephyrin, and contribute to the reduction in surface $GABA_A$ receptors. Because we found that GABARAPL2 may also be involved in $GABA_A$ receptor trafficking, we next performed immunoprecipitation experiments to examine the GABARAPL2-gephyrin interaction. We found that GABARAPL2 does interact with gephyrin in the brain but, more importantly, observed a significant reduction in the relative amount of coimmunoprecipitated gephyrin from *Atg7* cKO brains (Fig. 4F and

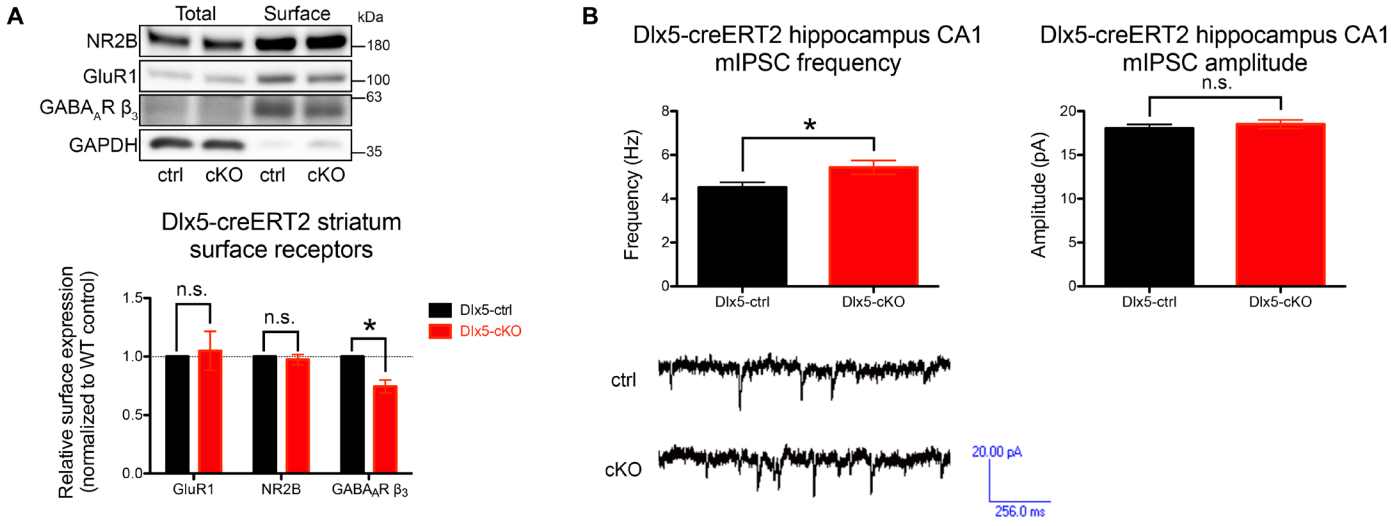

Fig. 3. Autophagy deficiency led to a reduction of surface GABA$_A$ receptors and increased GABA release by *Atg7* cKO GABAergic interneurons. (**A**) Significant reductions in surface expression of GABA$_A$ receptors (GABA$_A$R) were observed in striata of Dlx5-creERT2 *Atg7* cKO mice (see fig. S3A). $n = 4$ animals per genotype. (**B**) mIPSCs recorded from CA1 pyramidal cells in Dlx5-creERT2 *Atg7* cKO hippocampi showed a significant increase in frequency (left) but no differences in amplitude (right). Representative traces are shown at the bottom. $n = 35$ cells recorded from five different animals. Data are presented as means ± SEM. * $P < 0.05$, paired (A) or unpaired (B) two-tailed Student's *t* test.

fig. S4E). Similar to *Atg7* cKO brains, we observed by immunofluorescence in *Atg7* cKO neurons that GABARAPL2 is mislocalized to p62$^+$ aggregates (Fig. 4G and fig. S4F), with reduced localization to the trans-Golgi network (TGN, as marked by TGN38) compared to control neurons (Fig. 4H). Together, these data revealed that GABARAPL2 is involved in GABA$_A$ receptor trafficking, and this function was disrupted in autophagy-deficient neurons as it had mislocalized to p62$^+$ aggregates, away from the TGN.

Because GABARAPL2 appears to have a physiological role in mediating GABA$_A$ receptor trafficking and this function may be compromised in autophagy-deficient neurons, we attempted to replenish the functional protein pool in *Atg7* cKO neurons via GABARAPL2 overexpression and reverse the reduction of surface GABA$_A$ receptor expression. Because ectopically expressed GABARAPL2 was likely to interact with and be sequestered by p62$^+$ aggregates in a manner similar to the endogenous protein, we instead used an N-terminal truncation mutant of GABARAPL2 lacking its first eight amino acids (GABARAPL2 ΔN), corresponding to a region in LC3 critical for interactions with p62 (fig. S4G) (*25*). After confirmation that the N-terminal deletion similarly disrupts the interaction between GABARAPL2 and p62 (fig. S4H), we attempted to rescue the reduced surface expression of GABA$_A$ receptors in *Atg7* cKO neurons by overexpression of GABARAPL2 ΔN (fig. S4I). While *Atg7* cKO neurons with Venus overexpression in parallel showed a significant reduction in GABA$_A$ receptors, GABARAPL2 ΔN overexpression resulted in no significant difference between *Atg7* cKO and control neurons (Fig. 4I). Together, these results demonstrated that the loss of GABARAPL2 functions was causal for the reduced GABA$_A$ receptor trafficking in *Atg7* cKO neurons.

Conversely, a number of other proteins including BIG-2 (ARFGEF2) and NSF are also known to be involved in GABA$_A$ receptor trafficking. We next examined whether autophagy deficiency led to the mistrafficking of GABA$_A$ receptors by specifically affecting GABARAPs or via a more general effect involving other proteins in the process as well. By both immunofluorescence and immunoblotting experiments, we observed that BIG-2 and NSF did not mislocalize to p62$^+$ aggregates (fig. S5, A and B) or accumulate in *Atg7* cKO neurons or brain homogenates like p62 and GABARAPs (fig. S5, C and D). When we examined the localization of GABA$_A$ receptors with BIG-2 (primarily in the TGN of both *Atg7* cKO and control neurons), we observed large clusters of GABA$_A$ receptors colocalized with BIG-2$^+$ structures in *Atg7* cKO neurons not present in controls (Fig. 4J), consistent with our hypothesis that GABA$_A$ receptors may accumulate at the TGN when functions of GABARAPs are disrupted.

The findings described above suggest that the reduced surface expression of GABA$_A$ receptors observed in autophagy-deficient neurons is primarily due to a partial loss of function of GABARAPs as a result of formation of high–molecular weight species and/or sequestration by p62$^+$ aggregates. We investigated whether endosomal/lysosomal trafficking of GABA$_A$ receptors may have been altered due to the disruption of autophagic signaling to examine its potential contributions to the reduction of surface GABA$_A$ receptors. Immunofluorescence analyses of the subcellular localization of GABA$_A$ receptors in various endosomal (Rab5$^+$, Rab11$^+$, or Rab7$^+$ endosomes) and lysosomal (LAMP-1$^+$) compartments in *Atg7* cKO and control neurons suggested that only a minor population (10 to 15%) of GABA$_A$ receptors reside in these compartments and that this localization was not altered by autophagy deficiency (fig. S6, A to D). Thus, the reduction of surface GABA$_A$ receptors in *Atg7* cKO neurons was not associated with any changes in their endocytic flux.

Excessive p62 accumulation in autophagy-deficient and mTOR-hyperactivated neurons results in reduced GABA$_A$ receptor surface expression due to mislocalized GABARAPs

We next asked whether the observed disruption of GABA$_A$ receptor trafficking is specific to autophagy-deficient conditions or is due to a general increase in p62 levels. First, by immunofluorescence, we found that p62 overexpression in WT neurons led to the formation

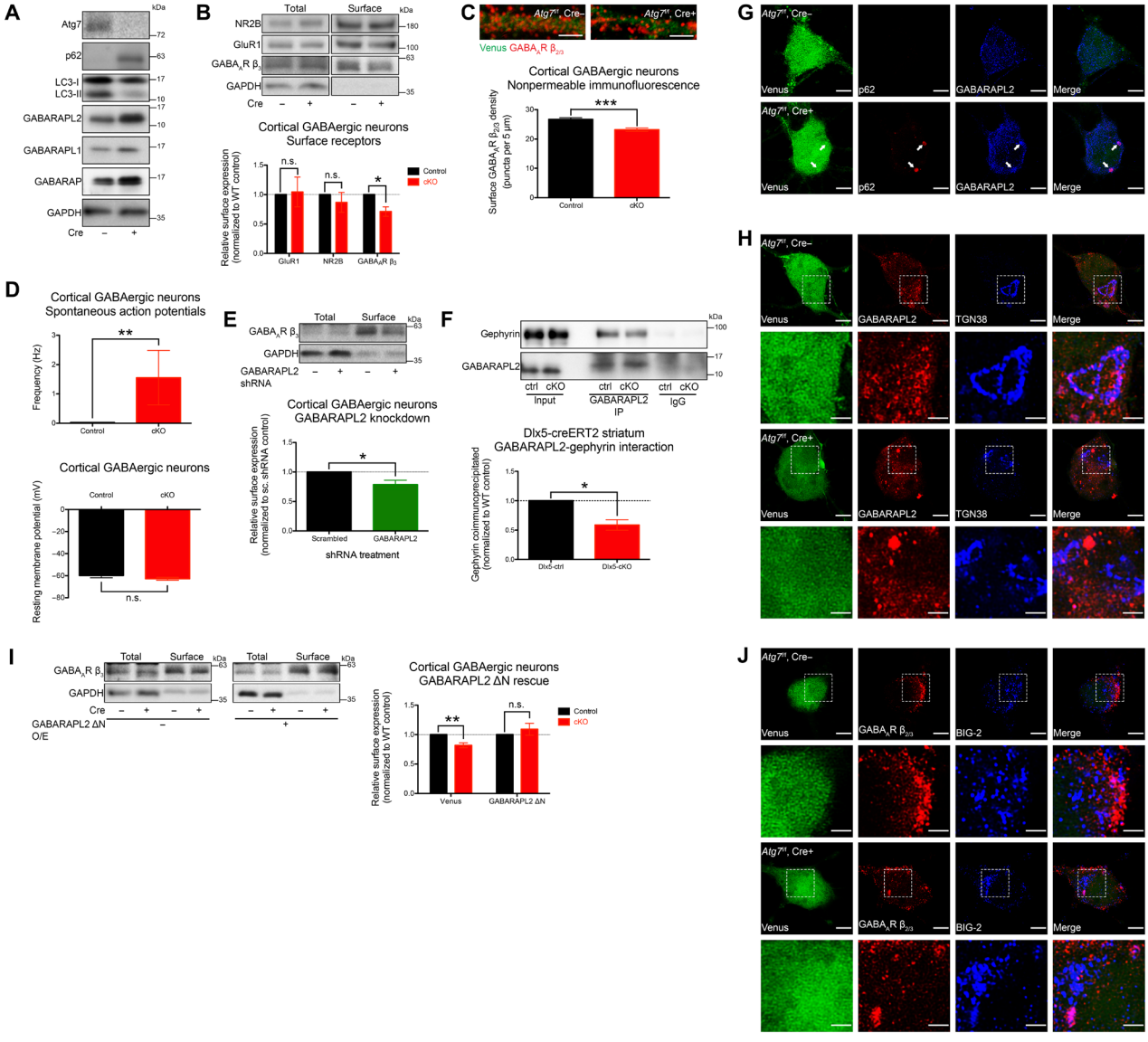

Fig. 4. GABA$_A$ receptor trafficking was disrupted by alterations of GABARAPL2 due to autophagy deficiency. (**A**) *Atg7* deletion in cultured cortical GABAergic interneurons (DIV15) derived from the MGEs of *Atg7*$^{flox/flox}$ embryos followed by infection with lentivirus expressing Venus reporter with or without Cre recombinase. Disrupted LC3 processing and accumulations of p62 and GABARAPs were observed as a result of autophagy deficiency induced by *Atg7* deletion. (**B**) A significant reduction of surface GABA$_A$ receptors was observed in *Atg7* cKO cultured cortical GABAergic interneurons, whereas NMDA and AMPA receptors were unchanged in both total and surface fractions. $n = 4$ independent experiments using distinct preparations of primary cultured neurons. (**C**) Immunofluorescence under nonpermeable conditions showed a significant reduction of surface GABA$_A$ receptors in *Atg7* cKO cultured cortical GABAergic interneurons. Venus expression (green fluorescence) was used as an indicator of infected neurons. $n = 30$ cells analyzed per genotype. (**D**) A significant increase in the frequency of spontaneous action potentials fired by *Atg7* cKO cultured cortical GABAergic interneurons was observed compared to controls (top). $n > 25$ cells per genotype; data shown for $n = 10$ and 9 cells for control and *Atg7* cKO, respectively, from three distinct preparations of primary cultured neurons, which fired spontaneous action potentials. Resting membrane potential was not altered by *Atg7* deletion in cultured cortical GABAergic interneurons (bottom). $n > 30$ cells per genotype from three distinct preparations of primary cultured neurons. (**E**) *Gabarapl2* knockdown in WT cultured cortical GABAergic interneurons resulted in a significant reduction of surface GABA$_A$ receptors. $n = 3$ independent experiments using distinct preparations of primary cultured neurons. (**F**) GABARAPL2-gephyrin interaction was significantly reduced in the brains of Dlx5-creERT2 (striatum) *Atg7* cKO mice (see fig. S4D). Quantifications shown represent the amount of gephyrin coimmunoprecipitated normalized by total gephyrin and amount of GABARAPL2 immunoprecipitated from individual samples. $n = 3$ independent experiments using tissue homogenates from distinct animals. (**G**) GABARAPL2 was mislocalized to p62$^+$ aggregates formed in *Atg7* cKO cultured cortical GABAergic interneurons in a similar manner as in affected neurons of *Atg7* cKO brains. (**H**) GABARAPL2 was observed by immunofluorescence to localize to the TGN marked by TGN38 in controls, but this localization was reduced in *Atg7* cKO cultured cortical GABAergic interneurons as the protein became mislocalized into foci. Venus signal was reduced in merge images to allow better visualization of signals from other channels. (**I**) GABARAPL2 ΔN overexpression (O/E) reversed the reduction of surface GABA$_A$ receptors observed in *Atg7* cKO cultured cortical GABAergic interneurons. $n = 5$ independent experiments using distinct preparations of primary cultured neurons. (**J**) Intracellular accumulations of GABA$_A$ receptors were observed in BIG-2$^+$ structures of *Atg7* cKO cultured cortical GABAergic interneurons but not in controls. Data are presented as means ± SEM. *$P < 0.05$, **$P < 0.01$, ***$P < 0.001$, paired (B, E, F, and I) or unpaired (C) two-tailed Student's *t* test or Kolmogorov-Smirnov test (D). Scale bars, 2 μm (C), 5 μm (G), 5 μm (H and J), and 2 μm (insets).

of $p62^+$ aggregates that also sequestered GABARAPs (Fig. 5A and fig. S7, A to C). Second, we observed a significant reduction in surface $GABA_A$ receptors in WT neurons with p62 overexpression (Fig. 5B). Third, if the reduced surface expression of $GABA_A$ receptors was caused by sequestration of GABARAPs by p62, a reduction of p62 in *Atg7* cKO neurons would be expected to restore such deficits. To test this hypothesis, we performed surface receptor biotinylation experiments on *Atg7* cKO and control neurons with or without *Sqstm1* (p62) knockdown. Consistent with our prediction, *Sqstm1* knockdown in *Atg7* cKO neurons reversed the reduction of surface $GABA_A$ receptors to control levels (Fig. 5C). Together, this series of experiments suggests that the pathologic accumulation of p62 in *Atg7* cKO neurons sequesters GABARAPs and disrupts the normal functions of GABARAPs, resulting in a reduction of surface $GABA_A$ receptor levels.

While we have demonstrated that pathologic p62 accumulation in autophagy-deficient neurons affects GABA signaling via a disruption of GABARAP functions, we questioned whether this pathogenic mechanism may have even broader implications. It was previously reported that *Tsc1* heterozygous excitatory neurons are hyperexcitable in a cell-autonomous manner due to a specific reduction in inhibitory input (*26*). As the Tsc1/2 complex is known to negatively regulate mTOR via the guanosine triphosphate (GTP)–binding protein Rheb and, in turn, promotes autophagic signaling, we asked whether the reported reduction of inhibitory input due to the derepression of mTOR activity (*26*) may have resulted from the mechanism described here. To address this question, we tested whether mTOR hyperactivation in cortical excitatory neurons due to a disruption of Tsc1/2 signaling may also lead to a reduction of surface $GABA_A$ receptor expression. To achieve mTOR hyperactivation, we used an shRNA-mediated knockdown approach against the mTOR negative regulator Tsc2 in WT cultured cortical excitatory neurons (fig. S7D). Consistent with previous reports (*27*), mTOR hyperactivation due to *Tsc2* knockdown resulted in autophagy suppression, as indicated by increased p62 levels (fig. S7D). We revealed that similar to $p62^+$ aggregates formed in *Atg7* cKO neurons and WT neurons overexpressing p62, GABARAPs were recruited to the $p62^+$ aggregates formed in WT neurons with derepressed mTOR activity (Fig. 5D and fig. S7, E and F). Surface receptor biotinylation experiments revealed that *Tsc2* knockdown also resulted in a significant reduction of $GABA_A$ receptors in WT neurons (Fig. 5E). Together, our results suggest a general mechanism that autophagy suppression due to mTOR hyperactivation, similar to autophagy deficiency in the case of *Atg7* deletion, disrupts the trafficking of $GABA_A$ receptors via the sequestration of GABARAPs by $p62^+$ aggregates.

Increased aggregation of GABARAPs in postmortem ASD brain samples

Given that both Dlx5-creERT2 and CaMKII-cre *Atg7* cKO mice exhibited social interaction deficits, we sought to determine whether GABARAPs are affected in ASD patients. To this end, we examined the expression and solubility of GABARAP, GABARAPL1, and GABARAPL2 in frozen BA40 brain samples from age- and gender-matched ASD patients and controls. Significant increases of all three proteins in the detergent-insoluble (0.2% sarkosyl) fraction were observed in ASD patients compared to controls (Fig. 6, A and B) without any significant differences in total tissue homogenates (Fig. 6, A and C). Furthermore, we observed a trend for increased insoluble p62 and a significant reduction in TSC2 expression in ASD patients (Fig. 6, D and E). TSC2 expression was negatively correlated with the insoluble amounts of not only p62 but also GABARAP family proteins (Fig. 6, F to I). These results are consistent with previous reports that autophagy may be suppressed in at least a subpopulation of ASD patients (*4*, *28*), and that the function of GABARAPs in mediating $GABA_A$ receptor trafficking could also be compromised.

DISCUSSION

Previous studies have shown ~20 to 35% reductions in surface $GABA_A$ receptor expression in several disease-relevant brain regions in ASD patients (*29*), and these reductions have been demonstrated to cause significant deficits in inhibitory synaptic strength (*30*). However, the underlying molecular mechanisms therein have remained unclear. In this study, we have uncovered a previously unknown pathogenic role of excessive p62 accumulation in autophagy-deficient neurons, which, via the sequestration and mislocalization of GABARAPs, disrupts the trafficking of $GABA_A$ receptors to the cell surface. We have also demonstrated a novel physiological role for GABARAPL2 in $GABA_A$ receptor trafficking, which was previously reported to show no interaction with $GABA_A$ receptor γ2 subunit or gephyrin by yeast two-hybrid assay (*24*). However, using brain homogenates from *Atg7* cKO and control mice, we demonstrated not only that GABARAPL2 interacted with gephyrin but also that the interaction was reduced in *Atg7* cKO brains. Furthermore, the role of GABARAPL2 in $GABA_A$ receptor trafficking was confirmed by knockdown experiments in WT neurons. Thus, despite some sequence differences between the GABARAPs, all three proteins are likely to be involved in trafficking of $GABA_A$ receptors, which may explain why *Gabarap* deletion alone did not significantly affect surface $GABA_A$ receptor expression (*31*).

The present study indicates that the disruption of $GABA_A$ receptor trafficking due to the sequestration of GABARAPs may represent a general pathogenic mechanism that contributes to various neurodevelopmental and neuropsychiatric disorders associated with dysregulated mTOR. This convergence between GABA and mTOR signaling might offer a mechanistic explanation for long-standing unresolved observations that increased epileptic activity in human patients and mutant mice with mTOR hyperactivation can be reversed by pharmacologic mTOR inhibition. As we have demonstrated here, derepression of mTOR signaling due to reduced Tsc2 leads to a reduction of surface $GABA_A$ receptors expressed on the affected neurons, which may be the underlying mechanism for the reduced inhibitory inputs into *Tsc1* mutant neurons described previously (*26*).

Consistent with a reduction of surface $GABA_A$ receptors in autophagy-deficient neurons, we observed the affected GABAergic interneurons to be hyperactive and increased GABA release onto their postsynaptic target cells as a result of disinhibition from reduced inhibitory inputs. Conversely, the same p62/GABARAP-dependent pathogenic mechanism affecting $GABA_A$ receptor trafficking was observed when *Atg7* was deleted in excitatory neurons by CaMKII-cre and would consequently result in hyperactivity of those cells in a similar fashion, in line with previous observations that CaMKII-cre *Atg7* cKO mice are more prone to develop spontaneous epileptic seizures (*28*). Our present findings, together with previous studies, suggest that there is an overall disruption in the excitatory-inhibitory (E-I) balance of autophagy-deficient neurons. Several recent studies have shown that disturbances in E-I balance are causal to social interaction deficits associated with various neurodevelopmental and neuropsychiatric disorders (*15*, *16*). Thus, we surmise that the altered

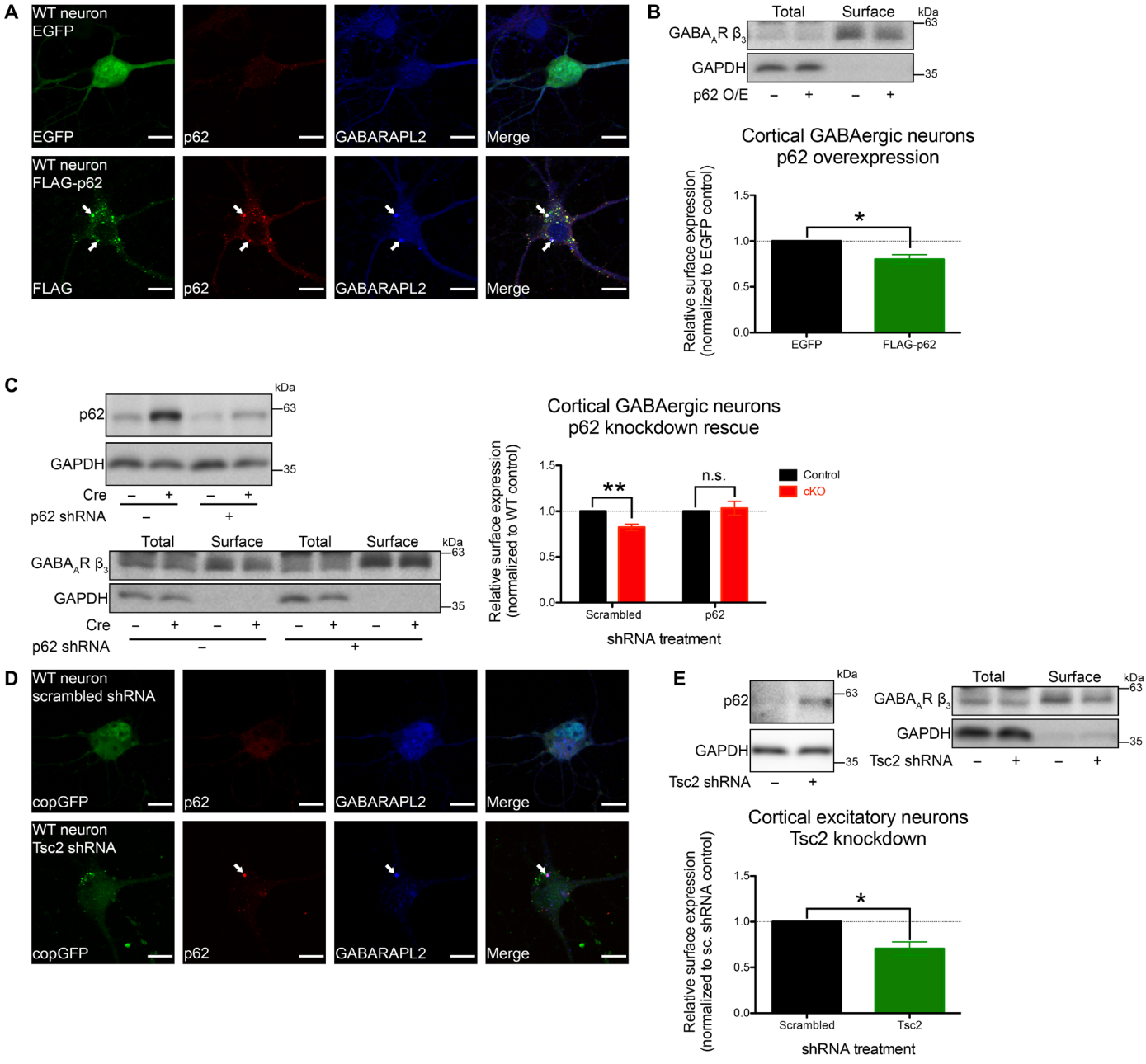

Fig. 5. Surface GABA$_A$ receptor expression depended on p62 levels. (**A**) p62 overexpression in WT cultured cortical GABAergic interneurons resulted in aggregates that recruited GABARAPL2 (see fig. S7, B and C). EGFP, enhanced green fluorescent protein. (**B**) p62 overexpression in WT cultured cortical GABAergic interneurons led to a significant reduction of surface GABA$_A$ receptors. $n = 3$ independent experiments using distinct preparations of primary cultured neurons. (**C**) *Sqstm1* knockdown in *Atg7* cKO cultured cortical GABAergic interneurons rescued the reduction in surface GABA$_A$ receptors. $n = 5$ independent experiments using distinct preparations of primary cultured neurons (**D**) mTOR hyperactivation via *Tsc2* knockdown in WT cultured cortical excitatory neurons resulted in p62$^+$ aggregates that sequestered GABARAPL2 (see fig. S7, E and F). (**E**) *Tsc2* knockdown resulted in a significant reduction of surface GABA$_A$ receptors in WT cultured cortical excitatory neurons. $n = 4$ independent experiments using distinct preparations of primary cultured neurons. Data are presented as means ± SEM. *$P < 0.05$, **$P < 0.01$, paired two-tailed Student's t test. Scale bars, 15 μm (A and D).

E-I balance, albeit in opposite directions by affecting either forebrain GABAergic interneurons or excitatory neurons, may have altered gamma oscillations or other types of network-level neurotransmission and caused the observed defects in social behaviors common to both *Atg7* cKO mice we have examined in this study (*32*).

Conversely, we note that social behavioral deficits appear to be more severe for CaMKII-cre *Atg7* cKO mice compared to Dlx5-cre *Atg7* cKO animals, as demonstrated by the social interaction preference index in the three-chamber social interaction test. This differential effect on social approach and novelty may be due to a difference

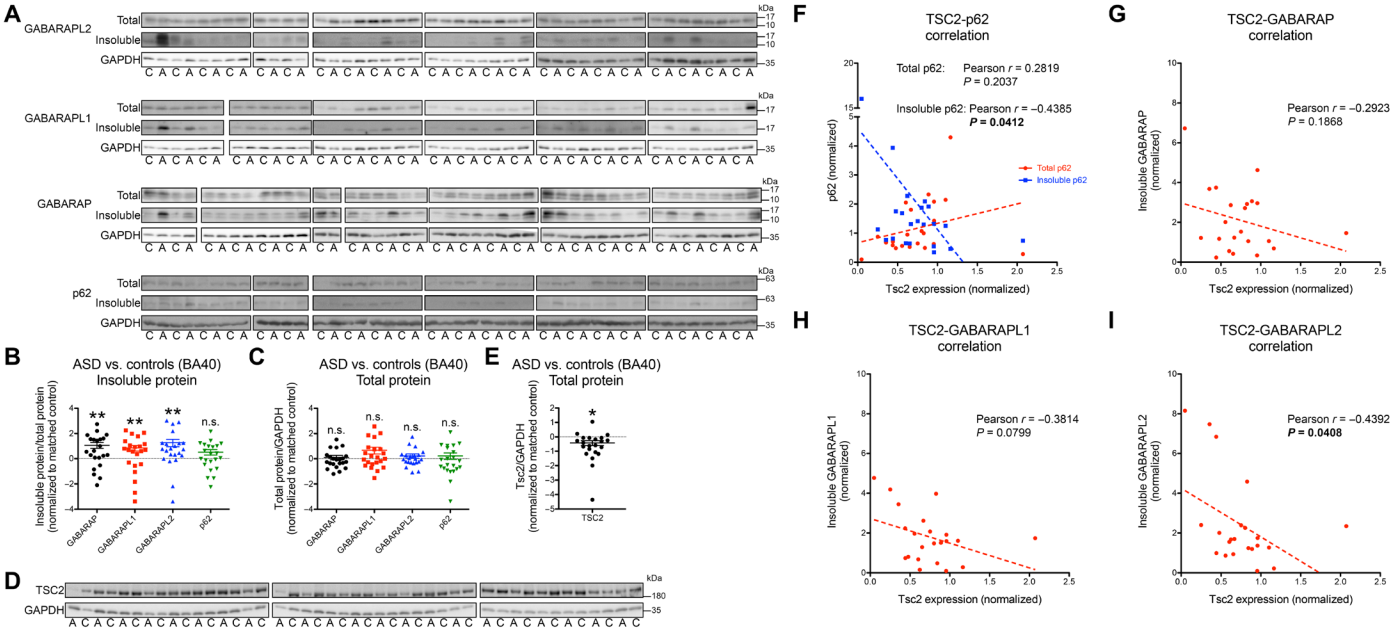

Fig. 6. Increased aggregation of GABARAPs in human ASD brain samples. (**A** to **C**) No significant difference was observed in total expression of GABARAPs between ASD and matched (age, sex, and ethnicity) control brains (BA40); however, significant increases in the detergent-insoluble fraction were observed for all three proteins. Insoluble p62 also showed a trend for increase in ASD brain samples. $n = 22$ pairs of ASD and matched controls. (**D** and **E**) A significant reduction in TSC2 expression was detected in ASD brain samples. $n = 22$ pairs of ASD and matched controls. (**F** to **I**) Negative correlations were observed between insoluble GABARAPs, insoluble p62, and TSC2 expression. No correlation with age was observed. Data are presented as means ± SEM. $^*P < 0.05$, $^{**}P < 0.01$, paired two-tailed Student's *t* test.

in the relative proportion of affected cells, as only about half of all cortical GABAergic interneurons were observed to form $p62^+$ aggregates in Dlx5-creERT2 *Atg7* cKO mice, while nearly all forebrain excitatory neurons affected by full or mPFC-specific CaMKII-cre *Atg7* deletion contained $p62^+$ aggregates (*4*, *17*, *28*). The difference is likely caused by a reduced recombination efficiency associated with age, as reported previously for Dlx5-creERT2 mice (*33*). In addition, we believe that other factors may have also contributed to this behavioral difference. First, overlapping but distinct regions of the forebrain were affected between Dlx5-creERT2 (cortex, hippocampus, and striatum) and CaMKII-cre (cortex and hippocampus). Second, the complex effect of deleting *Atg7* from distinct subclasses of GABAergic interneurons [some of which function to suppress the activity of other inhibitory neurons, thereby producing an overall disinhibition effect (*34*–*36*)] may have resulted in distinct outcomes at the network and behavioral level. Thus, while we have uncovered that autophagy is required in forebrain GABAergic interneurons for normal regulation of social behaviors, future studies using subclass-specific Cre mouse lines will provide additional insights into their distinct contributions to the behavioral phenotypes reported in our current study on Dlx5-creERT2 *Atg7* cKO mice.

The novel pathogenic mechanism we described here is distinct from that proposed previously concerning defective synaptic pruning in the developing brain as the primary cause of behavioral abnormalities due to autophagy deficiency (*4*, *12*). While our model does not preclude that both mechanisms can operate independently to contribute to the observed behavioral deficits, our results suggest that synaptic pruning deficits may play a secondary role in the observed pathology. Although *Atg7* deletion by Dlx5-creERT2 and mPFC-specific CaMKII-cre was initiated from adolescence, when most of the synaptic pruning had already occurred, both mice unexpectedly showed social deficits. Thus, our findings highlight the possibility that behavioral deficits arising from autophagy deficiency may not necessarily be related to specific defects during neurodevelopment per se, but rather a disruption in neurotransmission regardless of age. Local administration of the GABA antagonist bicuculline methiodide to WT animals after development to reduce GABA neurotransmission was previously shown to impair sociability (*37*). Together, our findings demonstrate that a disruption of GABA neurotransmission independent of defects during neurodevelopment may result in behavioral abnormalities including social deficits. While mutations contributing to neurodevelopmental and neuropsychiatric disorders in human patients may cause distinct neuronal deficits during and following neurodevelopment, their effects on mature neurons are rarely examined. It is important to note that several studies using mouse models of neurodevelopmental disorders have demonstrated that reexpression of the deleted genes after postnatal development can partially reverse neuronal and behavioral deficits (*38*, *39*). These findings suggest not only that neurodevelopmental defects can be reversed but also that the impairment of neuronal functions and behaviors in adolescence and adulthood is contributed by the loss of functional protein of interest in mature neurons.

In addition to the p62-dependent pathogenic mechanism described here, our experiments using human brain samples indicated that insoluble GABARAPs levels are increased in at least a subpopulation of ASD patients. In line with this observation, several genetic studies have previously identified deletions or microdeletions affecting *ATG7* (*40*) or *GABARAP* (*41*) in patients with ASD or ID, potentially implicating disrupted autophagy and altered GABARAPs as pathogenic factors. Furthermore, gene expression analyses using postmortem human brain samples of schizophrenics suggest possible deficits in autophagic signaling (*42*). Although it remains unclear whether GABARAPs are

directly involved, it was recently demonstrated that the trafficking of $GABA_A$ receptor subunits is altered in schizophrenic patients (*43*). Thus, our study offers a potential molecular mechanism for these previous reports using human brain samples. A recent study on *Ulk2* (*44*), an autophagic regulator previously shown to be partially duplicated in a single SZ patient, suggested an effect on GABA signaling and behavior in *Ulk2* heterozygous mice, although the deficits were attributed to an ambiguous mechanism specific to excitatory neurons in the PFC. We have demonstrated that the p62-dependent sequestration of GABARAPs affects both GABAergic interneurons and excitatory neurons in a similar manner to produce common behavioral abnormalities. Furthermore, our findings using *Tsc2* knockdown neurons provide broader implications for neurodevelopmental and neuropsychiatric disorders associated with mTOR dysregulation. Thus, this study provokes further studies on postmortem human brain samples for mTOR-related disorders to determine whether insoluble GABARAPs and disrupted autophagy may represent a more general defect affecting GABA neurotransmission and contribute to the manifestation of psychiatric symptoms.

METHODS

Animal care

All mice used were maintained on a C57BL/6J genetic background. Conditional deletion in forebrain GABAergic inhibitory neurons was achieved by genetic cross between $Atg7^{flox/flox}$ mice (*45*) and Dlx5-CreERT2 mice (*33*). Conditional *Atg7* deletion in forebrain excitatory neurons by CaMKII-cre (transgenic) was as previously described by Nilsson and colleagues (*17*). Genotypes of all animals were confirmed using polymerase chain reaction (PCR) from genomic tail DNA samples, as described previously (*17*, *33*). For Dlx5-creERT2 animals, $Atg7^{flox/+}$, $Dlx5^{creERT2/+}$ and $Atg7^{flox/flox}$, $Dlx5^{creERT2/+}$ were considered as Dlx5-control and cKO, respectively, to ensure equivalent gene dosages of Dlx5 in both genotypes (targeted mutation), whereas for CaMKII-cre animals, $Atg7^{flox/flox}$, Cre− and $Atg7^{flox/flox}$, Cre+ were considered as CaMKII-control and cKO, respectively. All experiments described were performed at 6 to 8 months after tamoxifen administration (Dlx5-creERT2) or 6 to 8 months of age (CaMKII-cre).

For CreERT2 induction, tamoxifen (2 μg per day) was administered by intraperitoneal injection during 8 and 10 weeks of age (four consecutive days during each week). Tamoxifen was first dissolved in ethanol (40 mg/ml) and subsequently in two volumes of canola oil. Ethanol was then removed in a centrifuge evaporator, resulting in a final tamoxifen concentration of 20 mg/ml. Dissolved tamoxifen was stored at −30°C until use and warmed to 37°C before injection.

Breeding of Dlx5-creERT2 animals was conducted using $Atg7^{flox/+}$, $Dlx5^{creERT2/+}$ males and $Atg7^{flox/flox}$, $Dlx5^{+/+}$ females or $Atg7^{flox/flox}$, $Dlx5^{+/+}$ males and $Atg7^{flox/+}$, $Dlx5^{creERT2/+}$ females. Neither parents were treated with tamoxifen. Breeding of CaMKII-cre animals was conducted using $Atg7^{flox/flox}$, Cre+ males and $Atg7^{flox/flox}$, Cre− females to avoid the possibility of abnormal rearing behaviors.

Preparation of primary neuronal cultures

Primary cortical GABAergic interneuron and excitatory neuron cultures were prepared from embryonic day 15 (E15) embryos (vaginal plug = E0) according to standard protocols. Briefly, $Atg7^{flox/flox}$ or WT embryos were dissected from pregnant dam, with cortex and MGE subdissected and pooled in ice-cold Hanks' balanced salt solution (HBSS). Dissected tissues were washed three times with ice-cold HBSS, followed by trypsinization for 15 min at 37°C. Trypsinization was terminated by the addition of equal volume of 10% fetal bovine serum (FBS)–Dulbecco's modified Eagle's medium (DMEM), and dissected tissues were triturated gently. Cell suspension was filtered through a 40-μm cell strainer to remove undigested tissues and plated onto polyethylenimine-coated cell culture plates or glass coverslips. Primary neuronal cultures were maintained in MACS Neuro Medium (130-093-570, Miltenyi Biotec Inc.) supplemented with MACS NeuroBrew-21 (130-093-566, Miltenyi Biotec Inc.), 0.5 mM GlutaMAX (35050061, Thermo Fisher Scientific Inc.), and 1% penicillin/streptomycin mix (09367-34, Nacalai Tesque Inc.) in a 37°C humidified incubator. All experiments were performed after 15 days in vitro (DIV15), with lentiviral infection performed on DIV0 for *Atg7* deletion by Cre recombinase expression or GABARAPL2 ΔN overexpression, DIV5 for p62 overexpression or *Tsc2* knockdown, and DIV10 for GABARAPL2 knockdown. For biochemical experiments, cells were plated on coated six-well plates at a density of 2.0×10^6 cells per well and infected with 20 to 25 μl of lentivirus per well. For immunofluorescence and electrophysiology experiments, cells were plated on coated glass coverslips at a density of 4.0×10^4 cells per well, maintained in 24-well plates, and infected with 1 μl of lentivirus per well.

Preparation of lentivirus

Lentivirus was produced by transfection of CSII-CMV-MCS-IRES2-Venus, CSII-CMV-Cre-HA-IRES2-Venus, CSII-CMV-FLAG-GABARAPL2 ΔN-IRES2-mRFP, CSII-CMV-FLAG-GABARAPL2 ΔN-IRES2-Cre-HA, CSII-CMV-FLAG-p62 plasmids, or pSIH1-copGFP/mRFP plasmids with shRNA sequences (table S1), with pCAG-HIVgp and pCAG-VSV-G plasmids into Lenti-X 293 T cells grown on 10-cm dishes and maintained in 8 ml of DMEM supplemented with 10% FBS and 1% penicillin/streptomycin mix at 37°C. Cultured medium was collected 2 days after transfection and filtered through a 0.45-μm syringe filter, and then lentivirus was precipitated using Lenti-X Concentrator (631232, Clontech Laboratories Inc.) according to the manufacturer's instructions. Precipitated lentivirus was resuspended in 250 μl of neuronal culture medium and kept at 4°C protected from light until use.

Preparation of AAV

AAV was produced by transfection of pAAV2-CaMKII promoter-MCS-IRES2-Venus or pAAV2-CaMKII promoter-CreHA-IRES2-Venus plasmids into AAV-293 cells with pAdΔF6 and pAAV2/1 plasmids. AAVs were purified by a discontinuous iodixanol gradient, as described previously (*46*). AAV titer was determined by quantitative PCR. Stereotaxic injections were bilaterally placed at 2.43 mm anterior to the bregma, 0.3 mm lateral to the sagittal suture, and 1.2 mm below the skull surface in 12-week-old CaMKII-cre $Atg7^{flox/flox}$ mice. One microliter of lentivirus (5.0×10^{12} genome copy/ml) was injected at a rate of 0.1 μl/min by a microinjector (Narishige).

Immunoblotting

Mouse brain regions of interest (i.e., striatum, cortex, and hippocampus) were homogenized in homogenization buffer containing 10 mM tris (pH 7.5), 500 mM NaCl, 10% sucrose, 1 mM EDTA, and a protease inhibitor mix (03969-34, Nacalai Tesque Inc.), followed by brief sonication. Tissue homogenates were centrifuged at 1500*g* for 5 min at 4°C to remove debris, with protein concentration measured using bicinchoninic acid (BCA) reagent (23227, Thermo Fisher Scientific

Inc.) using bovine serum albumin (BSA) as standard. Ten micrograms of total proteins per lane was separated by SDS-PAGE in precast 5 to 20% gradient acrylamide gels (2331730, Atto Corp.) and transferred to polyvinylidene difluoride (PVDF) membrane by semidry electrophoretic transfer. PVDF membranes were blocked using 1:1 mix of tris-buffered saline with 0.05% Tween 20 (TBS-T) and Blocking One (03953-95, Nacalai Tesque Inc.) and then incubated with primary antibodies diluted using TBS-T/Blocking One overnight with gentle agitation at 4°C overnight. PVDF membranes were washed three times with TBS-T and incubated with secondary antibodies using TBS-T/Blocking One for 2 hours with gentle agitation at 4°C. After incubation with secondary antibodies, PVDF membranes were washed three times with TBS-T. Antibodies were detected using luminol-based chemiluminescence assay kits [Chemi-Lumi One L (07880) or Chemi-Lumi One Ultra (11644), Nacalai Tesque Inc.] and ImageQuant LAS 3000 Mini (GE Healthcare). No manipulations other than global contrast and brightness adjustments were performed on gel images in Adobe Photoshop. Primary antibodies used in this study are listed in table S2.

Immunoprecipitation

Animals were anesthetized using phenobarbital and perfused transcardially with phosphate-buffered saline (PBS). Brains were removed, with cortex, hippocampus, and striatum subdissected and then flash-frozen using liquid nitrogen until experiment. Brain samples were homogenized as described above, and protein concentration was measured by BCA assay. Tissue homogenate (500 μg of total protein) was mixed in immunoprecipitation (IP) buffer containing 50 mM tris (pH 7.4), 150 mM NaCl, 1 mM $MgCl_2$, 1 mM EDTA, 1% NP-40, 0.25% SDS, and a protease inhibitor mix with either protein-specific antibody or whole immunoglobulin G (IgG) (both 1 μg) prebound to protein G magnetic beads (2 hours) at 4°C on a rotator for 2 hours. Protein G magnetic beads were then isolated by magnet and washed three times with IP buffer, followed by elution in SDS sample buffer, and boiled at 100°C for 10 min. Samples were analyzed by immunoblotting, as described above.

Native PAGE analysis

Tissue homogenates were prepared as described above, and protein concentration was measured by BCA assay. Ten micrograms of total protein was mixed with sample buffer and a final concentration of 1% sarkosyl or digitonin for analysis of GABARAPL2 and GABARAP, respectively. Samples were separated on NativePAGE 3-12% Bis-Tris gels and processed in the same manner as SDS-PAGE.

Sedimentation assay using postmortem human brain samples

Frozen postmortem human brain samples (BA40) were obtained via the National Institutes of Health (NIH) NeuroBioBank and stored at −80°C until use. Patient information provided by the NIH NeuroBioBank is listed in table S3. Frozen tissue samples were dissected to obtain approximately 50 mg of brain tissue, and tissue homogenates were generated as above for mouse brain tissues. Sarkosyl was added to each sample (500 μg of total proteins in 200 μl of total volume) for a 0.2% final concentration. The diluted protein samples were then incubated at 4°C for 30 min before ultracentrifugation at 100,000*g* for 1 hour at 4°C. Following ultracentrifugation, the supernatants were removed with the pellets resuspended and sonicated briefly in radioimmunoprecipitation assay (RIPA) buffer [50 mM tris (pH 7.4), 150 mM NaCl, 1% NP-40, 0.5% sodium deoxycholate, 0.1% SDS, and a protease inhibitor mix]. Proteins from total tissue homogenates and detergent-insoluble pellets were separated by SDS-PAGE as described above. All paired samples (paired by NIH NeuroBioBank for age, sex, and ethnicity) were loaded side by side for comparison in the order listed in table S3.

Immunofluorescence

Animals were anesthetized using phenobarbital and perfused transcardially with PBS. Brains were removed and immersion-fixed by 4% paraformaldehyde (PFA) overnight without subdissection. PFA immersion-fixed brain tissues were processed for either cryostat or paraffin sectioning. For cryostat sectioning, brain tissues were cryoprotected in PBS containing 30% sucrose overnight at 4°C and frozen in optimal cutting temperature (OCT) compound (4583, Sakura Finetek Japan Co. Ltd.). Frozen sections were cut at a thickness of 10 μm at −22°C and stored at −30°C until use after drying or as 30-μm floating sections transferred to PBS. Paraffin-embedded brain tissues were cut at a thickness of 7 μm and stored at room temperature until use. For some antibodies, antigen retrieval (0.1% Triton X-100 in 10 mM citric acetate, pH 6.0, at 121°C for 3 min) before blocking was required for optimal staining. Tissue sections were blocked with blocking solution (5% goat serum and 0.3% Tween 20 in PBS) for 30 min at 4°C and incubated with primary antibodies diluted in blocking solution overnight at 4°C. Following overnight incubation, tissue sections were washed three times with blocking solution followed by incubation with secondary antibodies diluted in blocking solution for 2 hours at 4°C. Tissue sections were washed three times with PBS and mounted using VECTASHIELD mounting medium with 4′,6-diamidino-2-phenylindole (DAPI) (H-1200, Vector Laboratories) or ProLong Diamond Antifade Mountant (P36965, Thermo Fisher Scientific Inc.) for observation by confocal microscopy (Nikon C2 si and Leica TCS SP8). Base images were captured and exported as TIFF files, and figures were created using Adobe Photoshop. Deconvolution was performed for some images using Huygens Professional (Scientific Volume Imaging). No manipulations other than global contrast and brightness adjustments were performed on the images obtained.

Nonpermeable immunofluorescence

For nonpermeable immunofluorescence experiments, procedures were similar to regular immunofluorescence as above, with the exception that both blocking and antibody incubations were performed in PBS with 5% goat serum only. Ten individual neurons, each from three independent preparations of cortical GABAergic interneurons, were used to derive the data presented. Between two and five distinct 10-μm segments from each neuron were randomly chosen and quantified for the number of nonpermeable immunofluorescence puncta, as detected by an antibody recognizing the extracellular domain of $GABA_A$ receptor $\beta_{2/3}$ subunit.

Surface receptor biotinylation

Primary neuronal cultures were washed twice with ice-cold PBS containing 0.5 mM $MgCl_2$ and 1 mM $CaCl_2$ (PBS/Mg^{2+}/Ca^{2+}). Surface proteins were biotinylated using EZ-Link sulfo-NHS-SS-biotin (0.25 mg/ml) (21331, Thermo Fisher Scientific Inc.) for 20 min at 4°C with gentle agitation. Neurons were washed three times with ice-cold PBS/Mg^{2+}/Ca^{2+} supplemented with 50 mM glycine and 0.5% BSA and twice with PBS/Mg^{2+}/Ca^{2+} before lysis by the addition

of RIPA buffer. Biotinylated proteins were enriched using streptavidin-conjugated magnetic beads (LSKMAGT10, EMD Millipore Co.) by mixing 50 μg of total proteins with 25 μl of magnetic beads. Streptavidin magnetic beads were washed three times using RIPA buffer after a 2-hour incubation period at 4°C on a rotator, and biotinylated proteins were eluted by heating the sample in SDS sample buffer for 10 min at 100°C. The eluted proteins were separated by SDS-PAGE and analyzed by immunoblotting, along with total lysate between treatment groups for comparison. In situ tissue surface protein biotinylation was performed using the same protocol except that freshly dissected tissue was biotinylated with sulfo-NHS-SS-biotin (1.0 mg/ml) for 45 min. The levels of surface biotinylated receptors were normalized by the levels of the receptor of interest and glyceraldehyde-3-phosphate dehydrogenase (GAPDH) in total lysate or homogenate and then compared across genotypes or treatment groups.

Semidenaturing detergent agarose gel electrophoresis and spike-in stable isotope labeling by amino acids in mammals

Animals were anesthetized at indicated ages using phenobarbital and perfused transcardially with PBS. Brains were removed, with cortex and hippocampus subdissected and flash-frozen using liquid nitrogen. Cortex and hippocampus were combined and homogenized in homogenization buffer, followed by brief sonication. Tissue homogenate was centrifuged at 1500*g* for 5 min to remove cell debris, and protein concentration was measured with BCA reagent using BSA as standard. Experimental tissue homogenate (1000 μg) was mixed with 500 μg of brain homogenate from mice fed with feed containing L-lysine ($^{13}C_6$) (MT-LYSC6-MB-PK, Cambridge Isotope Laboratories Inc.) for spike-in SILAM analysis. SDD-AGE sample buffer was added to the mixed sample and incubated at room temperature for 10 min before loading onto a 1.6% low melting point agarose gel (01146, Nacalai Tesque Inc.) containing 1% SDS in tris-acetate-EDTA (TAE) buffer. After electrophoresis in TAE buffer containing 0.1% SDS, the gel piece above 250 kDa was excised, melted, and digested by thermostable β-agarase (31107121, Nippon Gene Co.). Proteins in this "high–molecular weight" fraction were prepared for enzymatic digestion by using the filter-aided sample preparation, as described previously (*47*). The protein sample was digested overnight at 37°C using Lys-C, with digested peptides eluted from the filter by centrifugation. For MS, 2 μg of peptides was analyzed by liquid chromatography–electrospray ionization–MS/MS (LC-ESI-MS/MS).

Mass spectrometry

Protein analysis by LC-MS/MS

The enzymatically digested protein fragments were applied to a liquid chromatograph (EASY-nLC 1000; Thermo Fisher Scientific Inc.) coupled to a Q Exactive hybrid quadrupole-orbitrap mass spectrometer (Thermo Fisher Scientific Inc.) with a nanospray ion source in positive mode. The peptides derived from protein fragments were separated on a nano–high-performance liquid chromatography capillary column C18 (0.075 mm inside diameter × 150 mm length, 3 mm particle size, Nikkyo Technos Co. Ltd.). The mobile phase "A" was water with 0.1% formic acid, and the mobile phase "B" was acetonitrile with 0.1% formic acid. Two different slopes were used for a 60-min gradient at a flow rate of 300 ml/min: 5 to 35% B in 48 min, and then 35 to 65% B in 12 min. The Q Exactive MS was operated in top 10 data-dependent scan mode. The parameters of Q Exactive were as follows: spray voltage, 2.3 kV; capillary temperature, 275°C; mass range, 350 to 1800 *m/z* (mass/charge ratio); normalized collision energy, 28%. Raw data were acquired with Xcalibur software.

Protein identification

The MS and MS/MS data were searched against the Swiss-Prot database using Proteome Discoverer (Thermo Fisher Scientific Inc.) with the MASCOT search engine software (Matrix Science Inc.). The search parameters were as follows: enzyme, Lys-C protease static modifications, carbamidomethyl (Cys); dynamic modifications, oxidation (Met); precursor mass tolerance, ± 6 ppm (parts per million); fragment mass tolerance, ± 20 mDa; maximum missed cleavages, 1. The proteins were considered identified when their false discovery rates were less than 5%.

Behavioral tests

All behavioral tests were performed using male mice during the light cycle. For each genotype, at least two independent cohorts of mice were tested. All experiments and data analyses were performed in a blinded manner.

Open-field activity test

The experimental animal was placed in the center of an open-field apparatus (50 × 50 × 40 cm^3) illuminated by a light-emitting diode and allowed to move freely for 15 min. Parameters including distance traveled, time spent in the central area of the open field (30% of total area), and rearing time were measured every minute. Data were recorded and analyzed by using TimeOFCR4 (O'Hara & Co. Ltd.).

Resident-intruder social interaction test

The experimental animal was acclimated to its cage before the experiment. A distinct 6-week-old WT male DBA/2CrSlc (Japan SLC Inc.) was introduced to the experimental animal for a 10- or 5-min period for Dlx5-creERT2 and CaMKII-cre mice, respectively. Interaction between the animals was recorded using a digital video camera, with total contact time and number of contacts initiated by the experimental animal quantified.

Three-chamber social interaction test

The animal was first acclimated to the test apparatus made of clear fiberglass and consisted of three chambers with small entrances in between them for 10 min with objects in the opposing chambers. Following acclimatization, an unfamiliar mouse (stranger) and an object were introduced into opposing chambers, with the experimental mouse allowed to explore for an additional 10 min to evaluate the social approach. Social novelty was examined by replacing the object with a second unfamiliar mouse into the opposite chamber, with the experimental mouse allowed to explore for 10 min. The first stranger mouse was considered to be the familiar mouse in the last stage of the test. Time spent in each chamber was quantified and presented. Distinct 6-week-old WT male C57BL/6JJmsSlc mice (Japan SLC Inc.) were used as unfamiliar mice in this experiment. Time spent in the left and right chambers were compared for each genotype separately to examine social approach (object versus mouse) and social novelty (familiar versus stranger mouse), as detailed previously by Silverman and colleagues (*48*). The social interaction preference index was also calculated to compare across genotypes. This was defined as a percentage of the time in a selected chamber (e.g., chamber with mouse) relative to the total time spent in both chambers (e.g., sum of time in chamber with mouse and time in chamber with object). Therefore, the percentage of time in the selected chamber will be 50 if there is no preference.

Elevated plus maze test

The animal was placed in the center of a plus-shaped maze with two opposing ends lined by clear fiberglass (closed arms) and the two other ends without any barriers (open arms). The animal was allowed to move freely on the elevated maze for a period of 5 min. Parameters such as total distance traveled, distance traveled and time spent in open and closed arms, and time in center were measured. Data were recorded and analyzed by TimeEP2 (O'Hara & Co. Ltd.).

Tail suspension test

The experimental animal was suspended by holding its tail onto a force measurement apparatus for a 10-min period. The duration of immobility was recorded every minute. Data were recorded and analyzed by using TimeFZ2 (O'Hara & Co. Ltd.).

Nesting behavior test

Nesting behavior was examined and quantified according to the scoring system, as described previously (*49*). Briefly, mice were placed into individual cages with corncob bedding and a nestlet before the dark phase. Photos of the cages were taken every 12 hours for 2 or 3 days, and a score at each time point was assigned according to the rating scale.

Electrophysiology

Electrophysiology experiments were performed as described previously (*50*), with details provided below.

Slice preparation

Mice were deeply anaesthetized with halothane (2-bromo-2-chloro-1,1,1-trifluoroethane, Takeda Pharmaceutical Co. Ltd.) or isoflurane [(2RS)-2-chloro-2-(difluoromethoxy)-1,1,1-trifluoroethane, Pfizer Inc.] and sacrificed by decapitation. The whole brain was quickly removed into an ice-cold cutting solution comprising 200 mM sucrose, 4 mM KCl, 1 mM NaH_2PO_4, 0.2 mM $CaCl_2$, 10 mM $MgCl_2$, 26.2 mM $NaHCO_3$, 11 mM D-(+)-glucose, 0.1 mM L(+)-ascorbic acid, and 0.5 mM sodium pyruvate, saturated with 95% O_2 and 5% CO_2. Each brain hemisphere glued on a piece of agar block (4% in saline) was sliced along the longer axis of hippocampus at a thickness of 400 μm, using a microslicer (LinearSlicer Pro7, Dosaka EM Co. Ltd.). Hippocampi were dissected out of whole-brain slices and recovered in a submerged holding chamber filled with a physiological medium [artificial cerebrospinal fluid (aCSF)] comprising 119 mM NaCl, 2.5 mM KCl, 1 mM NaH_2PO_4, 2.5 mM $CaCl_2$, 1.3 mM $MgCl_2$, 26.2 mM $NaHCO_3$, 11 mM D-(+)-glucose, 0.1 mM L(+)-ascorbic acid, and 0.5 mM sodium pyruvate, continuously bubbled with 95% O_2 and 5% CO_2. The slices, which had been equilibrated for more than 2 hours, were transferred to an immersion-type recording chamber and superfused with well-bubbled aCSF at a rate of 2.5 ml/min. All physiological experiments were carried out at 25°C.

Patch clamp (acute hippocampal slices)

Whole-cell voltage clamp configuration was obtained by a blind access to CA1 pyramidal cell layer with a patch pipette (4 to 7 megohms, Harvard Apparatus). The composition of the pipette solution for EPSCs recording was the following: 122.5 mM Cs gluconate, 17.5 mM CsCl, 10 mM Hepes, 0.2 mM EGTA, 8 mM NaCl, 2 mM Mg-ATP, and 0.3 mM Na_3-GTP (pH 7.3; 290 to 300 mOsm). For IPSC recording, Cs gluconate was partially replaced with CsCl as follows: 40 mM Cs gluconate, 100 mM CsCl, 10 mM Hepes, 0.2 mM EGTA, 8 mM NaCl, 2 mM Mg-ATP, and 0.3 mM Na_3-GTP (pH 7.3; 290 to 300 mOsm). AMPA receptor– and NMDA receptor–mediated currents (AMPAR- and NMDAR-EPSCs) were recorded at −70 and +40 mV, respectively, in the presence of picrotoxin (100 μM) and CGP55845 (1 μM). NMDAR-EPSCs were recorded after pharmacologic isolation with 2,3-dihydroxy-6-nitro-7-sulfamoyl-benzo[f]quinoxaline (NBQX) (20 μM). Schaffer collateral fibers were surgically cut and stimulated at 0.1 Hz. The amplitude of the EPSC was analyzed for the comparison between genotypes. IPSCs mediated by $GABA_A$ receptors were recorded under blockade of NBQX (10 μM) and D-AP5 (25 μM). mEPSC and mIPSC were recorded at −70 mV in the presence of tetrodotoxin (TTX; 0.5 μM). Amplitude and frequency for miniature currents were analyzed using Mini Analysis Program version 6 (Synaptosoft Inc.) for the comparison between genotypes. Series resistances were less than 30 megohms, and there was no significant difference in series resistance between experimental groups. The monitored synaptic responses were filtered at 1 kHz using an Axon 200B or 700B amplifier and digitized at 10 kHz using Clampex software of pClamp 9 or 10 suite (Molecular Devices LLC). Membrane potentials in whole-cell patch clamp were represented without being compensated for liquid junction potential.

Patch clamp (primary cultured cortical GABAergic neurons)

Whole-cell patch-clamp recordings were carried out using DIV14 to 21 primary cortical GABAergic interneuron cultures placed on the stage of a Zeiss Axio Examiner upright microscope using Axopatch 200B and Multiclamp amplifiers (Axon Instruments). The recording chamber was continuously perfused with an extracellular solution containing 130 mM NaCl, 2.5 mM KCl, 2.2 mM $CaCl_2$, 1.5 mM $MgCl_2$, 10 mM D-glucose, and 10 mM Hepes (pH 7.35; osmolarity adjusted to 290 mOsm). The micropipettes were made from borosilicate glass capillaries, with a resistance in the range of 3 to 5 megohms. The intracellular solution contained 100 mM K-gluconate, 17 mM KCl, 5 mM NaCl, 5 mM $MgCl_2$, 10 mM Hepes, 0.5 mM EGTA, 4 mM ATPK2, and 0.5 mM GTP-Na (pH 7.3; osmolarity adjusted to 280 mOsm). All recordings were performed at room temperature (21° to 24°C). Data were recorded at 10 kHz and analyzed offline. All analysis was performed in Clampfit and Excel.

Drug

Drugs were purchased from the following sources: picrotoxin (28004-71, Nacalai Tesque Inc.; sc-202765, Santa Cruz Biotechnology Inc.), TTX (32775-51, Nacalai Tesque Inc.; 1078, Tocris Bioscience), CGP55845 (1248, Tocris Bioscience), D-AP5 (0106, Tocris Bioscience), and NBQX (0373, Tocris Bioscience).

Statistical analyses

The statistical significance of the data was examined by Student's *t* test or Kolmogorov-Smirnov test for comparisons between two groups, or by one-way analysis of variance (ANOVA) with Bonferroni's multiple comparison test for analyses of three or more groups using Microsoft Excel 16 or GraphPad Prism 6 unless otherwise indicated. Data are presented as means ± SEM. Results were considered statistically significant if $P < 0.05$.

Ethical considerations

All experimental procedures were in accordance with guidelines for animal care and human tissue sample use of RIKEN Center for Brain Science.

SUPPLEMENTARY MATERIALS

Supplementary material for this article is available at http://advances.sciencemag.org/cgi/content/full/5/4/eaau8237/DC1

Fig. S1. *Atg7* deletion in forebrain GABAergic neurons by Dlx5-creERT2.

Fig. S2. GABARAPs mislocalized to $p62^+$ aggregates in affected neurons of Dlx5-creERT2 and CaMKII-cre *Atg7* cKO mice.

Fig. S3. Autophagy deficiency led to a reduction of surface $GABA_A$ receptors but no change in excitatory signaling.
Fig. S4. Reduction of $GABA_A$ receptors in cortical GABAergic interneurons due to compromised functions of GABARAPL2 by autophagy deficiency.
Fig. S5. Levels and localizations of BIG-2 and NSF were not affected by autophagy deficiency.
Fig. S6. $GABA_A$ receptors are not substantially localized to endosomal and lysosomal compartments in cortical GABAergic interneurons and are not altered by autophagy deficiency.
Fig. S7. Reduced surface $GABA_A$ receptor expression by manipulation of p62 levels.
Table S1. shRNA sequences used in this study.
Table S2. Antibodies used in this study.
Table S3. Patient information for frozen postmortem human brain samples.

REFERENCE AND NOTES

1. M. Costa-Mattioli, L. M. Monteggia, mTOR complexes in neurodevelopmental and neuropsychiatric disorders. *Nat. Neurosci.* **16**, 1537–1543 (2013).
2. C. G. Gkogkas, A. Khoutorsky, I. Ran, E. Rampakakis, T. Nevarko, D. B. Weatherill, C. Vasuta, S. Yee, M. Truitt, P. Dallaire, F. Major, P. Lasko, D. Ruggero, K. Nader, J.-C. Lacaille, N. Sonenberg, Autism-related deficits via dysregulated eIF4E-dependent translational control. *Nature* **493**, 371–377 (2013).
3. E. Santini, T. N. Huynh, A. MacAskill, A. G. Carter, P. Pierre, D. Ruggero, H. Kaphzan, E. Klann, Exaggerated translation causes synaptic and behavioural aberrations associated with autism. *Nature* **493**, 411–415 (2013).
4. G. Tang, K. Gudsnuk, S.-H. Kuo, M. L. Cotrina, G. Rosoklija, A. Sosunov, M. S. Sonders, E. Kanter, C. Castagna, A. Yamamoto, Z. Yue, O. Arancio, B. S. Peterson, F. Champagne, A. J. Dwork, J. Goldman, D. Sulzer, Loss of mTOR-dependent macroautophagy causes autistic-like synaptic pruning deficits. *Neuron* **83**, 1131–1143 (2014).
5. S. Coghlan, J. Horder, B. Inkster, M. A. Mendez, D. G. Murphy, D. J. Nutt, GABA system dysfunction in autism and related disorders: From synapse to symptoms. *Neurosci. Biobehav. Rev.* **36**, 2044–2055 (2012).
6. S. H. Fatemi, A. R. Halt, J. M. Stary, R. Kanodia, S. C. Schulz, G. R. Realmuto, Glutamic acid decarboxylase 65 and 67 kDa proteins are reduced in autistic parietal and cerebellar cortices. *Biol. Psychiatry* **52**, 805–810 (2002).
7. A. A. Curley, D. Arion, D. W. Volk, J. K. Asafu-Adjei, A. R. Sampson, K. N. Fish, D. A. Lewis, Cortical deficits of glutamic acid decarboxylase 67 expression in schizophrenia: Clinical, protein, and cell type-specific features. *Am. J. Psychiatry* **168**, 921–929 (2011).
8. The Wellcome Trust Case Control Consortium, Genome-wide association study of 14,000 cases of seven common diseases and 3,000 shared controls. *Nature* **447**, 661–678 (2007).
9. S. Han, C. Tai, C. J. Jones, T. Scheuer, W. A. Catterall, Enhancement of inhibitory neurotransmission by $GABA_A$ receptors having $\alpha_{2,3}$-subunits ameliorates behavioral deficits in a mouse model of autism. *Neuron* **81**, 1282–1289 (2014).
10. P. Fazzari, A. V. Paternain, M. Valiente, R. Pla, R. Luján, K. Lloyd, J. Lerma, O. Marín, B. Rico, Control of cortical GABA circuitry development by Nrg1 and ErbB4 signalling. *Nature* **464**, 1376–1380 (2010).
11. C. Fu, B. Cawthon, W. Clinkscales, A. Bruce, P. Winzenburger, K. C. Ess, GABAergic interneuron development and function is modulated by the *Tsc1* gene. *Cereb. Cortex* **22**, 2111–2119 (2012).
12. H.-J. Kim, M.-H. Cho, W. H. Shim, J. K. Kim, E.-Y. Jeon, D.-H. Kim, S.-Y. Yoon, Deficient autophagy in microglia impairs synaptic pruning and causes social behavioral defects. *Mol. Psychiatry* **22**, 1576–1584 (2016).
13. M. Komatsu, S. Waguri, M. Koike, Y.-s. Sou, T. Ueno, T. Hara, N. Mizushima, J.-i. Iwata, J. Ezaki, S. Murata, J. Hamazaki, Y. Nishito, S.-i. Iemura, T. Natsume, T. Yanagawa, J. Uwayama, E. Warabi, H. Yoshida, T. Ishii, A. Kobayashi, M. Yamamoto, Z. Yue, Y. Uchiyama, E. Kominami, K. Tanaka, Homeostatic levels of p62 control cytoplasmic inclusion body formation in autophagy-deficient mice. *Cell* **131**, 1149–1163 (2007).
14. S. R. Yoshii, A. Kuma, T. Akashi, T. Hara, A. Yamamoto, Y. Kurikawa, E. Itakura, S. Tsukamoto, H. Shitara, Y. Eishi, N. Mizushima, Systemic analysis of *Atg5*-null mice rescued from neonatal lethality by transgenic ATG5 expression in neurons. *Dev. Cell* **39**, 116–130 (2016).
15. F. Wang, J. Zhu, H. Zhu, Q. Zhang, Z. Lin, H. Hu, Bidirectional control of social hierarchy by synaptic efficacy in medial prefrontal cortex. *Science* **334**, 693–697 (2011).
16. O. Yizhar, L. E. Fenno, M. Prigge, F. Schneider, T. J. Davidson, D. J. O'Shea, V. S. Sohal, I. Goshen, J. Finkelstein, J. T. Paz, K. Stehfest, R. Fudim, C. Ramakrishnan, J. R. Huguenard, P. Hegemann, K. Deisseroth, Neocortical excitation/inhibition balance in information processing and social dysfunction. *Nature* **477**, 171–178 (2011).
17. P. Nilsson, K. Loganathan, M. Sekiguchi, Y. Matsuba, K. Hui, S. Tsubuki, M. Tanaka, N. Iwata, T. Saito, T. C. Saido, Aβ secretion and plaque formation depend on autophagy. *Cell Rep.* **5**, 61–69 (2013).
18. D. S. Kryndushkin, I. M. Alexandrov, M. D. Ter-Avanesyan, V. V. Kushnirov, Yeast [*PSI*$^+$] prion aggregates are formed by small Sup35 polymers fragmented by Hsp104. *J. Biol. Chem.* **278**, 49636–49643 (2003).
19. S. Rayavarapu, W. Coley, E. Cakir, V. Jahnke, S. Takeda, Y. Aoki, H. Grodish-Dressman, J. K. Jaiswal, E. P. Hoffman, K. J. Brown, Y. Hathout, K. Nagaraju, Identification of disease specific pathways using in vivo SILAC proteomics in dystrophin deficient *mdx* mouse. *Mol. Cell. Proteomics* **12**, 1061–1073 (2013).
20. H. Weidberg, E. Shvets, T. Shpilka, F. Shimron, V. Shinder, Z. Elazar, LC3 and GATE-16/GABARAP subfamilies are both essential yet act differently in autophagosome biogenesis. *EMBO J.* **29**, 1792–1802 (2010).
21. T. A. Leil, Z.-W. Chen, C.-S. S. Chang, R. W. Olsen, $GABA_A$ receptor-associated protein traffics $GABA_A$ receptors to the plasma membrane in neurons. *J. Neurosci.* **24**, 11429–11438 (2004).
22. E. S. Lein, M. J. Hawrylycz, N. Ao, M. Ayres, A. Bensinger, A. Bernard, A. F. Boe, M. S. Boguski, K. S. Brockway, E. J. Byrnes, L. Chen, L. Chen, T.-M. Chen, M. Chi Chin, J. Chong, B. E. Crook, A. Czaplinska, C. N. Dang, S. Datta, N. R. Dee, A. L. Desaki, T. Desta, E. Diep, T. A. Dolbeare, M. J. Donelan, H.-W. Dong, J. G. Dougherty, B. J. Duncan, A. J. Ebbert, G. Eichele, L. K. Estin, C. Faber, B. A. Facer, R. Fields, S. R. Fischer, T. P. Fliss, C. Frensley, S. N. Gates, K. J. Glattfelder, K. R. Halverson, M. R. Hart, J. G. Hohmann, M. P. Howell, D. P. Jeung, R. A. Johnson, P. T. Karr, R. Kawal, J. M. Kidney, R. H. Knapik, C. L. Kuan, J. H. Lake, A. R. Laramee, K. D. Larsen, C. Lau, T. A. Lemon, A. J. Liang, Y. Liu, L. T. Luong, J. Michaels, J. J. Morgan, R. J. Morgan, M. T. Mortrud, N. F. Mosqueda, L. L. Ng, R. Ng, G. J. Orta, C. C. Overly, T. H. Pak, S. E. Parry, S. D. Pathak, O. C. Pearson, R. B. Puchalski, Z. L. Riley, H. R. Rockett, S. A. Rowland, J. J. Royall, M. J. Ruiz, N. R. Sarno, K. Schaffnit, N. V. Shapovalova, T. Sivisay, C. R. Slaughterbeck, S. C. Smith, K. A. Smith, B. I. Smith, A. J. Sodt, N. N. Stewart, K.-R. Stumpf, S. M. Sunkin, M. Sutram, A. Tam, C. D. Teemer, C. Thaller, C. L. Thompson, L. R. Varnam, A. Visel, R. M. Whitlock, P. E. Wohnoutka, C. K. Wolkey, V. Y. Wong, M. Wood, M. B. Yaylaoglu, R. C. Young, B. L. Youngstrom, X. F. Yuan, B. Zhang, T. A. Zwingman, A. R. Jones, Genome-wide atlas of gene expression in the adult mouse brain. *Nature* **445**, 168–176 (2007).
23. H. Wang, F. K. Bedford, N. J. Brandon, S. J. Moss, R. W. Olsen, $GABA_A$-receptor-associated protein links $GABA_A$ receptors and the cytoskeleton. *Nature* **397**, 69–72 (1999).
24. M. Kneussel, S. Haverkamp, J. C. Fuhrmann, H. Wang, H. Wässle, R. W. Olsen, H. Betz, The γ-aminobutyric acid type A receptor ($GABA_AR$)-associated protein GABARAP interacts with gephyrin but is not involved in receptor anchoring at the synapse. *Proc. Natl. Acad. Sci. U.S.A.* **97**, 8594–8599 (2000).
25. E. Shvets, E. Fass, R. Scherz-Shouval, Z. Elazar, The N-terminus and Phe52 residue of LC3 recruit p62/SQSTM1 into autophagosomes. *J. Cell Sci.* **121**, 2685–2695 (2008).
26. H. S. Bateup, C. A. Johnson, C. L. Denefrio, J. L. Saulnier, K. Kornacker, B. L. Sabatini, Excitatory/inhibitory synaptic imbalance leads to hippocampal hyperexcitability in mouse models of tuberous sclerosis. *Neuron* **78**, 510–522 (2013).
27. A. Di Nardo, M. H. Wertz, E. Kwiatkowski, P. T. Tsai, J. D. Leech, E. Greene-Colozzi, J. Goto, P. Dilsiz, D. M. Talos, C. B. Clish, D. J. Kwiatkowski, M. Sahin, Neuronal Tsc1/2 complex controls autophagy through AMPK-dependent regulation of ULK1. *Hum. Mol. Genet.* **23**, 3865–3874 (2014).
28. J. McMahon, X. Huang, J. Yang, M. Komatsu, Z. Yue, J. Qian, X. Zhu, Y. Huang, Impaired autophagy in neurons after disinhibition of mammalian target of rapamycin and its contribution to epileptogenesis. *J. Neurosci.* **32**, 15704–15714 (2012).
29. A. L. Oblak, T. T. Gibbs, G. J. Blatt, Reduced $GABA_A$ receptors and benzodiazepine binding sites in the posterior cingulate cortex and fusiform gyrus in autism. *Brain Res.* **1380**, 218–228 (2011).
30. Y. Ge, Y. Kang, R. M. Cassidy, K.-M. Moon, R. Lewis, R. O. L. Wong, L. J. Foster, A. M. Craig, Clptm1 limits forward trafficking of $GABA_A$ receptors to scale inhibitory synaptic strength. *Neuron* **97**, 596–610.e8 (2018).
31. G. A. O'Sullivan, M. Kneussel, Z. Elazar, H. Betz, GABARAP is not essential for $GABA_A$ receptor targeting to the synapse. *Eur. J. Neurosci.* **22**, 2644–2648 (2005).
32. W. Cao, S. Lin, Q.-q. Xia, Y.-l. Du, Q. Yang, M.-y. Zhang, Y.-q. Lu, J. Xu, S.-m. Duan, J. Xia, G. Feng, J. Xu, J.-h. Luo, Gamma oscillation dysfunction in mPFC leads to social deficits in neuroligin 3 R451C knockin mice. *Neuron* **97**, 1253–1260.e7 (2018).
33. H. Taniguchi, M. He, P. Wu, S. Kim, R. Paik, K. Sugino, D. Kvitsani, Y. Fu, J. Lu, Y. Lin, G. Miyoshi, Y. Shima, G. Fishell, S. B. Nelson, Z. J. Huang, A resource of Cre driver lines for genetic targeting of GABAergic neurons in cerebral cortex. *Neuron* **71**, 995–1013 (2011).
34. W. Zhang, L. Zhang, B. Liang, D. Schroeder, Z.-w. Zhang, G. A. Cox, Y. Li, D.-T. Lin, Hyperactive somatostatin interneurons contribute to excitotoxicity in neurodegenerative disorders. *Nat. Neurosci.* **19**, 557–559 (2016).
35. H. Xu, H.-Y. Jeong, R. Tremblay, B. Rudy, Neocortical somatostatin-expressing GABAergic interneurons disinhibit the thalamorecipient layer 4. *Neuron* **77**, 155–167 (2013).
36. C. K. Pfeffer, M. Xue, M. He, Z. J. Huang, M. Scanziani, Inhibition of inhibition in visual cortex: The logic of connections between molecularly distinct interneurons. *Nat. Neurosci.* **16**, 1068–1076 (2013).

37. T. A. Paine, N. Swedlow, L. Swetschinski, Decreasing GABA function within the medial prefrontal cortex or basolateral amygdala decreases sociability. *Behav. Brain Res.* **317**, 542–552 (2017).
38. Y. Mei, P. Monteiro, Y. Zhou, J.-A. Kim, X. Gao, Z. Fu, G. Feng, Adult restoration of *Shank3* expression rescues selective autistic-like phenotypes. *Nature* **530**, 481–484 (2016).
39. Y. Sztainberg, H.-m. Chen, J. W. Swann, S. Hao, B. Tang, Z. Wu, J. Tang, Y.-W. Wan, Z. Liu, F. Rigo, H. Y. Zoghbi, Reversal of phenotypes in *MECP2* duplication mice using genetic rescue or antisense oligonucleotides. *Nature* **528**, 123–126 (2015).
40. C. S. Poultney, A. P. Goldberg, E. Drapeau, Y. Kou, H. Harony-Nicolas, Y. Kajiwara, S. De Rubeis, S. Durand, C. Stevens, K. Rehnström, A. Palotie, M. J. Daly, A. Ma'ayan, M. Fromer, J. D. Buxbaum, Identification of small exonic CNV from whole-exome sequence data and application to autism spectrum disorder. *Am. J. Hum. Genet.* **93**, 607–619 (2013).
41. C. M. B. Carvalho, S. Vasanth, M. Shinawi, C. Russell, M. B. Ramocki, C. W. Brown, J. Graakjaer, A.-B. Skytte, A. M. Vianna-Morgante, A. C. V. Krepischi, G. S. Patel, L. Immken, K. Aleck, C. Lim, S. W. Cheung, C. Rosenberg, N. Katsanis, J. R. Lupski, Dosage changes of a segment at 17p13.1 lead to intellectual disability and microcephaly as a result of complex genetic interaction of multiple genes. *Am. J. Hum. Genet.* **95**, 565–578 (2014).
42. M. R. Barnes, J. Huxley-Jones, P. R. Maycox, M. Lennon, A. Thornber, F. Kelly, S. Bates, A. Taylor, J. Reid, N. Jones, J. Schroeder, C. A. Scorer, C. Davies, J. J. Hagan, J. N. C. Kew, C. Angelinetta, T. Akbar, S. Hirsch, A. M. Mortimer, T. R. E. Barnes, J. de Belleroche, Transcription and pathway analysis of the superior temporal cortex and anterior prefrontal cortex in schizophrenia. *J. Neurosci. Res.* **89**, 1218–1227 (2011).
43. T. M. Mueller, C. E. Remedies, V. Haroutunian, J. H. Meador-Woodruff, Abnormal subcellular localization of $GABA_A$ receptor subunits in schizophrenia brain. *Transl. Psychiatry* **5**, e612 (2015).
44. A. Sumitomo, H. Yukitake, K. Hirai, K. Horike, K. Ueta, Y. Chung, E. Warabi, T. Yanagawa, S. Kitaoka, T. Furuyashiki, S. Narumiya, T. Hirano, M. Niwa, E. Sibille, T. Hikida, T. Sakurai, K. Ishizuka, A. Sawa, T. Tomoda, *Ulk2* controls cortical excitatory–inhibitory balance via autophagic regulation of p62 and GABAA receptor trafficking in pyramidal neurons. *Hum. Mol. Genet.* **27**, 3165–3176 (2018).
45. M. Komatsu, S. Waguri, T. Chiba, S. Murata, J.-i. Iwata, I. Tanida, T. Ueno, M. Koike, Y. Uchiyama, E. Kominami, K. Tanaka, Loss of autophagy in the central nervous system causes neurodegeneration in mice. *Nature* **441**, 880–884 (2006).
46. S. Zolotukhin, B. J. Byrne, E. Mason, I. Zolotukhin, M. Potter, K. Chesnut, C. Summerford, R. J. Samulski, N. Muzyczka, Recombinant adeno-associated virus purification using novel methods improves infectious titer and yield. *Gene Ther.* **6**, 973–985 (1999).
47. J. R. Wiśniewski, A. Zougman, N. Nagaraj, M. Mann, Universal sample preparation method for proteome analysis. *Nat. Methods* **6**, 359–362 (2009).
48. J. L. Silverman, M. Yang, C. Lord, J. N. Crawley, Behavioural phenotyping assays for mouse models of autism. *Nat. Rev. Neurosci.* **11**, 490–502 (2010).
49. R. M. J. Deacon, Assessing nest building in mice. *Nat. Protoc.* **1**, 1117–1119 (2006).
50. H. Matsukawa, S. Akiyoshi-Nishimura, Q. Zhang, R. Luján, K. Yamaguchi, H. Goto, K. Yaguchi, T. Hashikawa, C. Sano, R. Shigemoto, T. Nakashiba, S. Itohara, Netrin-G/NGL complexes encode functional synaptic diversification. *J. Neurosci.* **34**, 15779–15792 (2014).

Acknowledgments: We thank members of the Laboratory for Protein Conformation Diseases, S. Itohara, and C. Yokoyama for discussion, as well as H. Fujimura and N. Takahashi for technical assistance. We thank M. Komatsu for providing the p62 expression plasmid. We are grateful to the Support Unit for Bio-Material Analysis in RIKEN CBS's Research Resources Division for technical help with MS sample analysis, DNA sequencing, and FANTOM clone distribution. Postmortem human brain samples used in this study were obtained via the NIH NeuroBioBank, specifically the University of Maryland Brain and Tissue Bank, which provided the samples. **Funding:** This work was supported by Grant-in-Aid for Scientific Research on Innovative Areas from Japan Society for the Promotion of Science (26116044 to M.T. and JP18dm0107083 to T.Y.), RIKEN Pioneering Projects, Cellular Evolution (M.T.), the RIKEN Cellular Evolution project (M.T.), the Strategic Research Program for Brain Sciences from the Japan Agency for Medical Research and Development (JP18H05435 to T.Y.), RIKEN CBS/BSI internal funds (Y.G. and M.T.), the Postdoctoral Fellowship Program for Foreign Researchers from Japan Society for the Promotion of Science (23-01512 to K.K.H.), and the RIKEN Foreign Postdoctoral Researcher program (K.K.H.). **Author contributions:** K.K.H. and M.T. conceived experiments, wrote the manuscript, and secured funding. K.K.H., N.T., A.W., T.E.C., H.M., and Y.N.-M. performed the experiments. P.N. and T.C.S. provided *Atg7* floxed mice, expertise, and feedback. R.E., Y.G., and T.Y. provided expertise and feedback. **Competing interests:** The authors declare that they have no competing interests. **Data and materials availability:** All data needed to evaluate the conclusions in the paper are present in the paper and/or the Supplementary Materials. Additional data related to this paper may be requested from the authors.

Submitted 18 July 2018
Accepted 20 February 2019
Published 10 April 2019
10.1126/sciadv.aau8237

Citation: K. K. Hui, N. Takashima, A. Watanabe, T. E. Chater, H. Matsukawa, Y. Nekooki-Machida, P. Nilsson, R. Endo, Y. Goda, T. C. Saido, T. Yoshikawa, M. Tanaka, GABARAPs dysfunction by autophagy deficiency in adolescent brain impairs $GABA_A$ receptor trafficking and social behavior. *Sci. Adv.* **5**, eaau8237 (2019).